Parametric Study of Radiator Concepts for a Stirling Radioisotope Power System Applicable to Deep Space Missions

Albert J. Juhasz, Roy C. Tew, and Lanny G. Thieme
Glenn Research Center, Cleveland, Ohio

Since its founding, NASA has been dedicated to the advancement of aeronautics and space science. The NASA Scientific and Technical Information (STI) Program Office plays a key part in helping NASA maintain this important role.

The NASA STI Program Office is operated by Langley Research Center, the Lead Center for NASA's scientific and technical information. The NASA STI Program Office provides access to the NASA STI Database, the largest collection of aeronautical and space science STI in the world. The Program Office is also NASA's institutional mechanism for disseminating the results of its research and development activities. These results are published by NASA in the NASA STI Report Series, which includes the following report types:

- TECHNICAL PUBLICATION. Reports of completed research or a major significant phase of research that present the results of NASA programs and include extensive data or theoretical analysis. Includes compilations of significant scientific and technical data and information deemed to be of continuing reference value. NASA's counterpart of peer-reviewed formal professional papers but has less stringent limitations on manuscript length and extent of graphic presentations.

- TECHNICAL MEMORANDUM. Scientific and technical findings that are preliminary or of specialized interest, e.g., quick release reports, working papers, and bibliographies that contain minimal annotation. Does not contain extensive analysis.

- CONTRACTOR REPORT. Scientific and technical findings by NASA-sponsored contractors and grantees.

- CONFERENCE PUBLICATION. Collected papers from scientific and technical conferences, symposia, seminars, or other meetings sponsored or cosponsored by NASA.

- SPECIAL PUBLICATION. Scientific, technical, or historical information from NASA programs, projects, and missions, often concerned with subjects having substantial public interest.

- TECHNICAL TRANSLATION. English-language translations of foreign scientific and technical material pertinent to NASA's mission.

Specialized services that complement the STI Program Office's diverse offerings include creating custom thesauri, building customized data bases, organizing and publishing research results . . . even providing videos.

For more information about the NASA STI Program Office, see the following:

- Access the NASA STI Program Home Page at *http://www.sti.nasa.gov*

- E-mail your question via the Internet to help@sti.nasa.gov

- Fax your question to the NASA Access Help Desk at 301–621–0134

- Telephone the NASA Access Help Desk at 301–621–0390

- Write to:
  NASA Access Help Desk
  NASA Center for AeroSpace Information
  7121 Standard Drive
  Hanover, MD 21076

Parametric Study of Radiator Concepts for a Stirling Radioisotope Power System Applicable to Deep Space Missions

Albert J. Juhasz, Roy C. Tew, and Lanny G. Thieme
Glenn Research Center, Cleveland, Ohio

Acknowledgments

The work was performed in part under Interagency Agreement SAA 3–198 with DOE.

Contents

Parametric Study of Radiator Concepts for Stirling Radioisotope Power System Applicable to Deep Space Missions

Albert J. Juhasz, Roy C. Tew, and Lanny G. Thieme
National Aeronautics and Space Administration
Glenn Research Center
Cleveland, Ohio 44135

Summary

The Department of Energy (DOE) and the NASA Glenn Research Center are developing a Stirling converter for an advanced radioisotope power system to provide spacecraft onboard electric power for NASA deep space missions. This high-efficiency converter is being evaluated as an alternative to replace the much lower efficiency radioisotope thermoelectric generator (RTG). The current power requirement (6 years after beginning of mission (BOM) for a mission to Jupiter) is 210 W_e (watts electric) to be generated by two separate power systems, one on each side of the spacecraft. Both two-converter and four-converter system designs are being considered, depending on the amount of required redundancy.

The Stirling converter cycle reject heat is transferred to space via a lightweight radiator. The design and performance of the radiator have a significant impact on the performance and overall mass of the power system. Also, radiator reliability is important for achieving high overall system reliability. In the study reported herein, NASA Glenn evaluated a number of different radiator concepts. Two different ways of transporting heat to the radiator fins were considered: heat pipes and simple thermal conduction through solid material having high thermal conductivity. The heat-pipe concepts are subdivided into optimal and fixed heat-pipe locations. The heat-pipe radiators are in the plane of the converter axes of symmetry, whereas the no-heat-pipe radiators are perpendicular to the plane of the converter axes. Four types of material were considered for the radiator fins: aluminum (Al), beryllium (Be), carbon composite (C-C), and thermal pyrolytic graphite (TPG). The TPG must be encapsulated in another material for strength; TPG encapsulants considered in the study were aluminum, beryllium, and carbon composite.

These conceptual radiator evaluations were done with GPHRAD (general purpose heat (source power system) radiator), a dedicated radiator analysis tool recently developed at NASA Glenn. It is a finite-difference computational code developed for the analysis and design of circular sector radiators for radioisotope Stirling space power systems. The code includes a novel subroutine (TSCALC) to determine equilib-rium space sink temperatures anywhere in the Solar System and is based, in part, on the radiator surface characteristics.

For a nominal 105-W_e power system, total radiator masses were as low as 1.75 kg for no-heat-pipe disk radiator designs and as low as 2.17 kg for heat-pipe designs. As the design layouts went from the more complex (heat-pipe radiators with heat pipes requiring a number of bends) to the simpler (simple disks and no heat pipes), the benefits of using radiator fins made of highly conductive TPG increased. However, designs with aluminum, beryllium, and carbon composites were also attractive in terms of mass and thermal performance for each potential layout. It should be noted that aluminum is a common radiator material, beryllium is a material that requires careful processing to avoid inhalation of beryllium dust, and carbon composites are just beginning to be used for space radiators. In contrast, TPG needs substantial development before it can be ready for this type of application.

The better no-heat-pipe radiators are lighter and have outer radii that are two-thirds as large as the better heat-pipe designs. However, the best no-heat-pipe designs (based on low mass and good thermal performance) require the use of TPG fins. The no-heat-pipe concept requires that the power system be mounted farther from the spacecraft to maximize the radiator view to space. For scoping purposes, a view factor of 1.5 was used for both the heat-pipe and no-heat-pipe evaluations. For final spacecraft layout, both radiator concepts will need to be iteratively evaluated on the basis of view factors determined by ray-tracing techniques. Ground-based vibration tests should reveal whether the disk radiators may also need to be connected by tie-rods at different circumferential locations to minimize resonance with launch vibrations.

Introduction

The Department of Energy (DOE) and the NASA Glenn Research Center are developing a Stirling converter for an advanced radioisotope power system to provide spacecraft onboard electric power for NASA deep space missions. This high-efficiency converter is being evaluated as an alternative to
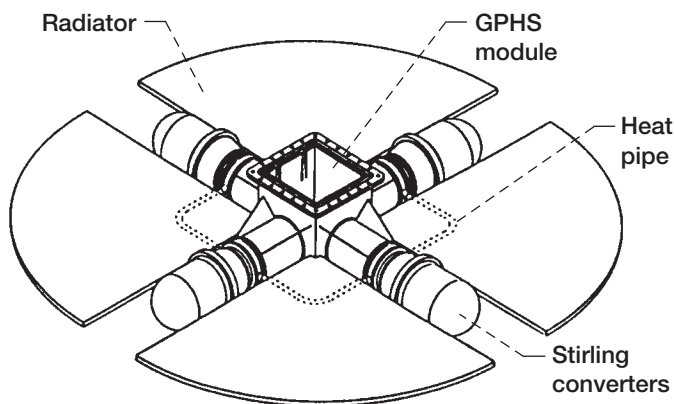
Figure 1.—Orbital Sciences Corporation system concept (ref. 4).

Overall size: 25 cm long by 8.3 cm in diam
Projected converter flight weight: 1.7 kg
Design life: 100 000 + hr

Figure 2.—55-W_e prototype converter.

replace the much lower efficiency radioisotope thermoelectric generator (RTG). With the efficiency of the Stirling power system exceeding 20 percent, this alternative will reduce the necessary isotope inventory by a factor of at least 3 compared with RTG's. Stirling is the most developed converter option of the advanced power concepts under consideration (refs. 1 and 2).

Orbital Sciences Corporation (OSC) has developed conceptual designs and completed system studies for the Stirling power system (refs. 3 and 4). A sketch of one Stirling four-converter concept is shown in figure 1 (most cases studied here were two-converter systems). The power system utilizes radioisotope general purpose heat source (GPHS) modules and opposed pairs of free-piston Stirling converters. The low-grade nonconvertible heat is rejected to space via a lightweight radiator using copper (Cu) water heat pipes and carbon-carbon (C-C) panels in a circular sector configuration. The current system power requirement (6 years after beginning of mission (BOM) for a mission to Jupiter) is 210 W_e to be generated by two separate systems, one on each side of the spacecraft. Both two-converter and four-converter system designs are being considered, depending on the amount of required redundancy.

The department of energy is developing the prototype Stirling converter under contract with Stirling Technology Company (STC) of Kennewick, WA (refs. 5 and 6). Two 55-W_e converters are now being tested at STC in a dynamically balanced opposed arrangement. The prototype converter is shown in figure 2. The design of the 55-W_e Stirling prototype is based on previous successful STC development efforts, particularly those for the 10-W_e radioisotope terrestrial converter (RG–10) and the 350-W_e RG–350 aimed at commercial cogeneration and remote power applications (ref. 7). NASA Glenn is providing technical consultation for this effort under an interagency agreement with DOE.

The design and performance of lightweight space radiators has a significant impact on the performance and overall mass of the power system as a whole. In previous work, lightweight, high-thermal-conductivity C-C radiator panels were fabricated
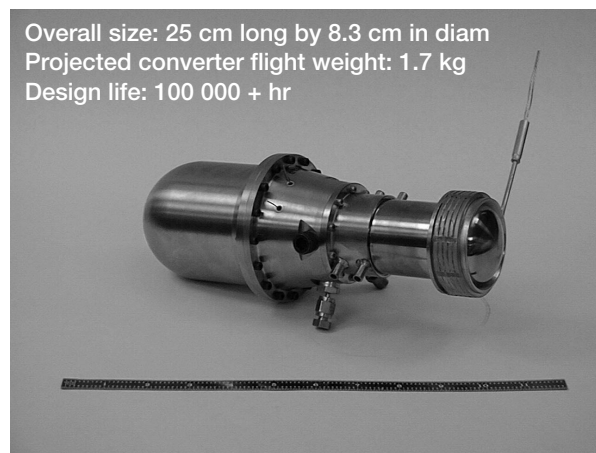
in small-scale laboratory heat-pipe test articles for Glenn for the SP–100 program (refs. 8 to 10). In the study reported herein, Glenn evaluated high-thermal-conductivity carbon and graphite heat-pipe and no-heat-pipe radiator concepts. Comparisons were made to radiators using aluminum and beryllium panels. This evaluation was done with a dedicated radiator analysis tool (GPHRAD, General Purpose Heat (Source Power System) Radiator), recently developed at Glenn. The study results are presented in the body of the report and a brief discussion of the code capabilities and options is given in appendix A.

Radiator Requirements

The radiator requirements for a Stirling radioisotope deep space mission were taken as follows for the purpose of conducting this study:

1. The radiator will be either directly coupled to the Stirling converter or coupled through a heat transport system, such as a heat pipe.

2. The cold-end temperature of the converter will be selected to maximize specific power of the system and is expected to be in the range of 373 to 423 K. The DOE/STC 55-W_e prototype converter was designed for a cold-end temperature of 393 K.

3. The radiator will be designed to reject the necessary heat over the entire mission profile from Earth to the deep space destination (e.g., Pluto or Jupiter) and maintain the converter cold-end temperature at its selected design value or lower. The current system concept assumes two power systems, one on each side of the spacecraft; each power system is required to produce 105 W_e 6 years after BOM for a Jupiter mission. Each power system is now expected to have two Stirling converters (unlike the four-converter OSC concept shown in figure 1) and to use two GPHS modules. The BOM heat input for each power system is assumed to be 486 W_t (watts thermal), 243 W_t per GPHS module. The nominal cycle reject heat for each power

system is 371 W_t at BOM and 354 W_t after 6 years for a Stirling converter with a 393 K cold-end temperature.

4. The radiator lifetime will be at least 15 years (based on a Pluto mission).

5. For each radiator concept, the goal will be to maximize system specific power (i.e., system power per unit system mass).

Description of Conceptual Radiator Design Study

The radiator computer code used in this study is described in appendixes A and B and was used to study both heat-pipe and no-heat-pipe disk radiator concepts for a Stirling radioisotope power system. The heat-pipe disk radiator concept was similar to the OSC system concept shown in figure 1. However, based on a more recent system layout, a two-converter concept was the primary focus of the study instead of the four-converter concept shown in figure 1. With the two-converter concept, two 180° circular sector radiator panels were used instead of the four 90° panels shown with the four converters in figure 1. Several four-converter, four-radiator-panel designs were analyzed. However, so that masses and radii could be directly compared with corresponding two-converter, two-panel designs, these comparisons are reported below.

The heat-pipe radiator concept studied was very similar to that seen in the exploded view of a radiator quadrant used in the OSC system concept (shown in fig. 3 with permission from OSC). Glenn did make four-converter projections to compare with OSC's to determine the level of agreement. This comparison did result in reasonable agreement but not all inputs could be matched to get a direct comparison (those comparisons are not reported here). Some of the input values for the present study were taken directly from OSC results. These values included the temperature drop that was assumed from the converter cold end through the heat pipe to the radiator fin root temperature and the mass of the copper saddles that were used to attach the heat pipe to the converter. However, there were differences in assumptions. For example, the sink temperature was calculated based on assumed coating properties and the view factor to space. Also, different values of thermal conductivity in the plane of the fin were assumed in this study for the carbon-carbon material. Finally, heat-pipe dimensions and geometry were different from those used by OSC.

Initial calculations were based on a circular 1-cm heat pipe, which was somewhat larger than that used by OSC. However, after conversations with Thermacore (a heat-pipe manufacturer), it was concluded that a larger 2-cm heat pipe was a safer choice for the design conditions and geometry being used. A square 2-cm heat pipe was chosen to provide less thermal resistance between the heat pipe and the fin surface than could be achieved with a circular heat pipe.

Fin materials used for the heat-pipe radiator concepts were pure aluminum (Al), carbon-carbon, beryllium (Be), and composites of each of these materials with thermal pyrolitic graphite (TPG) (ref. 11). Even though C-C is a composite itself, throughout the rest of this report, reference will be made to "pure" C-C to distinguish it from the composite of C-C and TPG. The TPG has excellent conductivity of 1700 W/m-K in two orthogonal directions but has only approximately 25 W/m-K in the third orthogonal direction. For radiator and electrical circuit board applications of TPG, the two high-conductivity orthogonal directions are typically in the plane of the radiator fin or the circuit board; the low-conductivity direction is typically perpendicular to the plane of the fin or board. Because TPG has little strength by itself, a thin layer of Al, C-C, or Be was used to encapsulate it. For all the TPG radiator studies carried out here, the thickness of the encapsulant was assumed to be about 0.5 mm. There was also assumed a TPG thickness below which fabrication would be difficult, about 0.7 mm, which corresponds to a 0.40 volume fraction of TPG based on about 0.5 mm of encapsulant. Therefore, the minimum thickness of TPG composite fin reported in this study was about 1.7 mm.

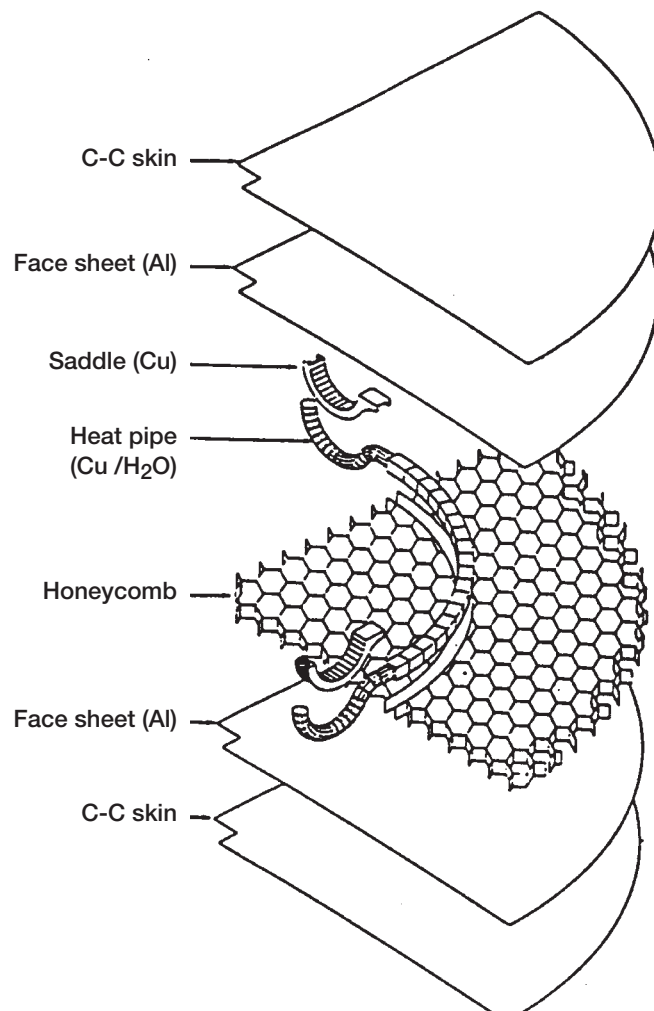Figure 3.—Exploded view of radiator quadrant used in Orbital Sciences Corporation system concept (ref. 2).

The labels in the figure, from top to bottom, read:
C-C skin
Face sheet (Al)
Saddle (Cu)
Heat pipe (Cu /H_2O)
Honeycomb
Face sheet (Al)
C-C skin

As long as the 1-cm heat pipe was under consideration, it appeared that by using a slightly "squashed" heat pipe (an elliptical cross section), there might be a benefit in using a tapered design such as that shown in figure 4 (with heat pipe embedded in solid material). However, when the heat-pipe size was increased to 2 cm, embedding the heat pipe in the TPG, even with tapering, resulted in a design that was too massive. Hence, with the chosen heat-pipe size, embedding the heat pipe in solid fin material was not a satisfactory solution. Therefore, only a double flat fin design was appropriate for the heat-pipe study, and the concept used was similar to that shown in figure 3. A 2-cm square heat pipe was embedded in 2-cm-thick aluminum honeycomb (assumed density of 0.128 g/cm^3). The honeycomb and heat pipe were then sand-wiched between two fins (of either pure material or TPG composite). The primary difference between this concept and that shown in figure 3 is that no face sheet was used between the honeycomb with an embedded heat pipe and the radiator fins. For Al, or TPG encapsulated in Al, no face sheet was needed. For Al honeycomb used in contact with other types of fin materials, there could be problems associated with joining and with differences in the coefficients of thermal expansion. In any case, to carry such a design beyond the conceptual stage, ther-mal stress analyses will be required to understand potential problems due to a CTE (coefficient of thermal expansion) mismatch of the Inconel 718 converter housing, the radiator fin material, and the copper heat pipes and saddles. Such problems would occur during startup and changes between operating conditions.

For most of the heat-pipe designs, the radial heat-pipe location was optimized to produce equal heat rejection from the areas of the radiator fin located inward and outward of the radial heat-pipe location. For relatively low fin thermal con-ductivity, such as that for the pure materials, this optimization significantly reduced the mass and radius of the radiator panels. Optimization had less impact on the higher conductivity TPG composites. Some runs with the heat-pipe location fixed at the
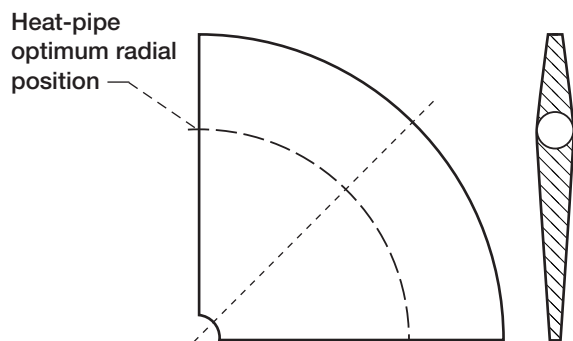
Stirling cold-end radial location of 14 cm were made for comparison and are reported in the Results and Discussion section. For the optimized designs, there must be bends in the heat pipe as it turns radially outward from the location of the Stirling cold-end heat exchanger and then bends back to its desired direction at the optimized radial location for the heat pipe. The mass of the heat pipe between these bends was neglected in this study.

A conceptual design study was also conducted on no-heat-pipe radiators for the same Stirling radioisotope deep space mission. The no-heat-pipe study was based on the concept shown in figure 5, in which the inner surface of a single 360° circular radiator fin is in contact with the outer cylindrical surface of the Stirling converter cold end; the radius of this surface is 2.4 cm. Therefore, the plane of the fin is disk shaped with a circular cutout for the converter. This concept could eliminate heat-pipe reliability concerns and significantly reduce the temperature drop from the converter cold end to the radiator fin root. For the heat-pipe radiator study, this temperature drop was assumed to be 15 K based on OSC's calculated results. For the no-heat-pipe study, it is estimated that the temperature drop across the contact surface between the converter cold end and the radiator should be no larger than 1 or 2 K; the reference temperature drop was assumed to be 2 K.

A more careful study will be needed to determine the overall relative impact of the two concepts (heat pipe and no-heat pipe) on system reliability. For example, the two concepts might have different sensitivities to structural vibrations and thermal stresses.

For the no-heat-pipe designs, flat and tapered surfaces were considered for the TPG composites and the C-C fins. Flat, tapered, and parabolic surfaces were considered for the pure metal (Al and Be) fins. The largest fin root thickness considered for the no-heat-pipe designs was 1 cm. The Stirling cold-end cylindrical surface is about 2 cm long. The GLIMPS (Globally Implicit Sterling) code was used to check the sensitivity of converter performance in maintaining the converter cold-end

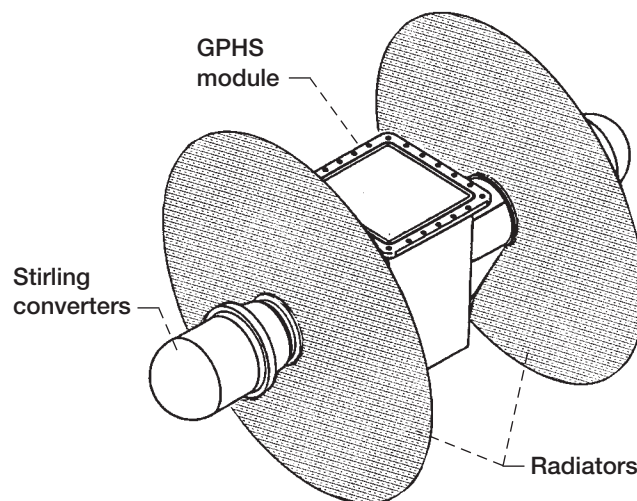Figure 4.—Heat pipe embedded in TPG inside tapered fin.

Figure 5.—No-heat-pipe radiator design concept.

temperature only in the middle third of the 2-cm length of the cold-end cylindrical surface. These GLIMPS simulations indicated that converter performance was not significantly affected by 10 K increases in the cold-end wall temperature on each side of the middle third of the cold-end surface. In any case, the design of a collar to be used as the interface between the Stirling cold end and the base of the no-heat-pipe radiator fin was roughed out to cover the entire 2-cm length of the cold-end surface. These calculations indicated that a collar weighing on the order of 0.1 kg would probably be adequate; this mass was included in the total mass of the no-heat-pipe designs.

The primary radiator surface coating used was Z–93, an inorganic paint that has high emissivity and low absorptivity. It is composed of zinc oxide pigment with a potassium silicate binder and has been used on various projects and is currently being used to coat Al radiator panels for the International Space Station.

Results and Discussion

The study results are reported in the approximate chronological order in which the study was done. Therefore, the reference case was the starting point. The Results and Discussion presents a comparison of the least-mass heat-pipe and no-heat-pipe radiator designs and is discussed in detail in the subsection Comparison of Heat-Pipe and No-Heat-Pipe Results. Table I also summarizes the results of the comparison.

Heat-Pipe Radiator Results

Aluminum/TPG reference case.—Aluminum/TPG radiators were analyzed for various volume fractions of TPG. The Al encapsulant was assumed to be 0.5-mm thick on each side of the TPG. The volume fraction of TPG was then assumed to be the TPG thickness divided by the total Al plus the TPG thickness. The contribution of the encapsulant at the inner and outer edges of the radiator fins was neglected in calculating the volume fraction; accounting for the encapsulant at the edges would slightly reduce the TPG volume fraction. The 2-cm square heat pipe was embedded in aluminum honeycomb. The heat pipe and honeycomb were sandwiched between two Al/TPG fins. This composite structure formed the circular sector Al/TPG heat-pipe radiator panels.

Reference sink temperature calculations using the TSCALC code were based on a Z–93 radiator surface coating with absorptivity α divided by emissivity ε, ($\alpha/\varepsilon = 0.18$ and $\varepsilon = 0.92$); the view factor to space F is 1.5; the insolation angle is ±30°; and the distance from the Sun is 0.9 astronomical units (AU). The corresponding reference sink temperature was 205.8 K. A view factor of 1 denotes that the equivalent of one side of the two-sided radiator is completely blocked from radiation and absorption and the equivalent of only one side has a completely unobstructed view of space. A view factor of 2 denotes that both sides of the radiator panel have an unobstructed view of space.

The reference radiator fin root temperature was assumed to equal a converter cold-end temperature of 393 K minus a 15 K temperature drop for the heat pipe and copper saddle, or 378 K. The reference heat rejection of 371 W_t corresponded to a system with two Stirling converters producing 115 W_e at the beginning of the mission near Earth (0.9 AU). The 371 W_t includes all thermal energy not converted to dc electric output, including the GPHS losses. The inner radius of the radiator panel was at 5 cm from the origin of the panel coordinates. The heat-pipe radial location was optimized to produce equal heat rejection in the radiator panel areas radially inward and outward from the heat-pipe location.

Aluminum conductivity and density are 173 W/m-K and 2.70 g/cm^3. The TPG conductivity in the plane of the fin is 1700 W/m-K and through the fin is 25 W/m-K. The TPG density is 2.26 g/cm^3. A composite conductivity was used in the plane of the fin based on the volume fractions of TPG and Al. The overall through-the-fin conductivity was assumed to equal to that of the TPG, 25 W/m-K.

Plots of heat-pipe radiator mass and outer radius are shown as functions of volume fraction of TPG in figure 6. For the same radiator runs, the total Al and TPG thickness (includes Al/TPG for fins on both sides of the honeycomb) and composite planar thermal conductivity are shown as a function of the volume fraction of TPG in figure 7. The temperature differences across the inner and outer radiator sectors are shown in figure 8 for the same runs.

It is seen in figure 6 that the minimum mass was found with pure Al (i.e., volume fraction of TPG = 0.0) and the minimum outer radius with a TPG volume fraction of 0.65. A TPG volume fraction of 0.20 gave results close to the minimum mass and radius; however, it was impractical to make the encapsulated TPG with such a small thickness of TPG. Therefore, a TPG volume fraction of 0.40 was chosen for use in the following sensitivity study. The outer radius for this run was very close to the minimum outer radius shown in figure 6; the radiator mass was about 0.5 kg larger than that for pure Al.
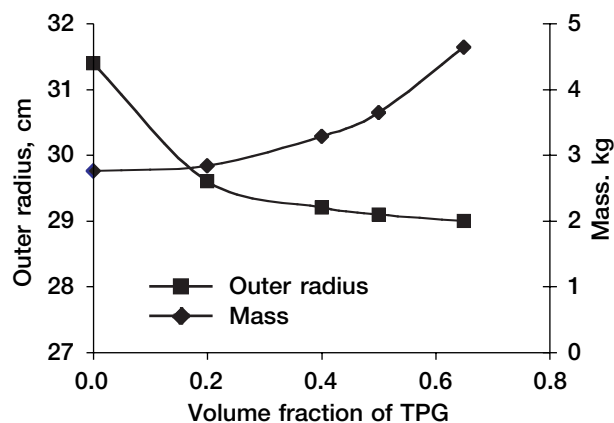

Figure 6.—Radiator mass and outer radius as functions of volume fraction of TPG for Al/TPG radiators.

TABLE I.—COMPARISON OF LEAST-MASS HEAT-PIPE AND NO-HEAT-PIPE DESIGNS FOR VARIOUS MATERIALS

[Z–93 coating (absorptivity/emissivity ratio, α/ε, 0.18; ε, 0.92); view factor, F, 1.5; distance from Sun, 0.9 AU; sink temperature, 205.8 K; converter cold-end temperature, 393 K; fin root temperature for heat-pipe case, 393 – 15 K = 378 K, and for no-heat-pipe case, 393 – 2K = 391 K; two-converter system; heat rejection, 371 W_t.]

Fin material	Mass, kg	Outer radius, cm	Power specific mass, kg/kW$_t$	Area specific mass, kg/m²	Thickness,[a] mm	Maximum temperature difference, K	Planar thermal conductivity, W/m-K	Through-the-plane thermal conductivity, W/m-K	Density, g/cm³	Fin area, m²	Power specific area, m²/kW
Optimized heat-pipe location											
Al	2.77	31.4	7.47	9.20	2.032	32.9	173	173	2.70	0.301	0.81
C-C	2.24	30.1	6.04	8.09	2.032	16.9	350	50	2.05	0.277	0.75
Be	2.17	30.8	5.85	7.46	2.032	26.3	220	220	1.80	0.291	0.78
Al/TPG40	3.28	29.2	8.84	12.57	3.386	4.6	784	25	2.52	0.261	0.70
Be/TPG40	2.80	29.2	7.55	10.73	3.386	4.5	812	25	1.98	0.261	0.70
C-C/TPG40	2.93	29.2	7.90	11.27	3.386	4.1	890	25	2.13	0.260	0.70
Fixed heat-pipe location (14 cm)											
Al	4.38	43.9	11.81	7.32	2.032	91.8	173	173	2.70	0.598	1.61
C-C	2.32	33.0	6.25	6.93	2.032	35.2	350	50	2.05	0.335	0.90
Be	2.59	37.6	6.98	5.95	2.032	63.6	220	220	1.80	0.435	1.17
Al/TPG40	3.20	29.8	8.63	11.81	3.386	8.4	784	25	2.52	0.271	0.73
C-C/TPG40	2.83	29.7	7.63	10.52	3.386	7.3	890	25	2.13	0.269	0.73
No heat pipe											
Al/TPG65	1.98	20.3	5.34	7.76	2.903	15.0	1166	25	2.41	0.255	0.69
C-C/TPG65	1.81	20.2	4.88	7.15	2.903	14.2	1228	25	2.19	0.253	0.68
Be/TPG65	1.75	20.2	4.72	6.89	2.903	14.8	1182	25	2.10	0.254	0.68
Al	4.01	27.4	10.81	8.53	Parabolic: 8 to 1	75.7	173	173	2.70	0.470	1.27
Be	2.20	27.6	5.93	4.64	Parabolic: 6 to 1	75.6	220	220	1.80	0.474	1.28
C-C	2.29	25.6	6.17	5.61	Tapered: 3 to 2	58.9	350	50	2.05	0.408	1.10
Be[b] reduced DT#1	2.46	23.4	6.63	7.19	Parabolic: 10 to 1	47.5	220	220	1.80	0.342	0.92
Be[b] reduced DT#2	3.18	22.0	8.57	10.56	Tapered: 10 to 1	34.3	220	220	1.80	0.301	0.81
TPG properties	- - -	- - -	- - -	- - -	- - - - - - - - -	- - -	1700	25	2.26	- - -	- - -

[a]Thickness is sum of thickness of both fins (on each side of Al honeycomb) for heat-pipe designs but is just thickness of one fin for no-heat-pipe designs.
[b]Reduced DT#1 and #2 denotes runs in which the thickness was increased, resulting in a reduction in temperature difference and size.
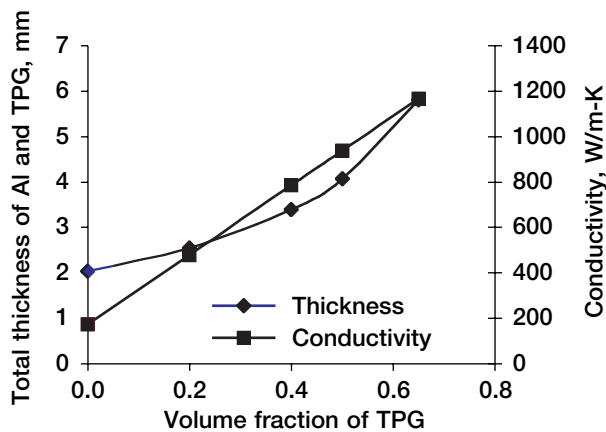
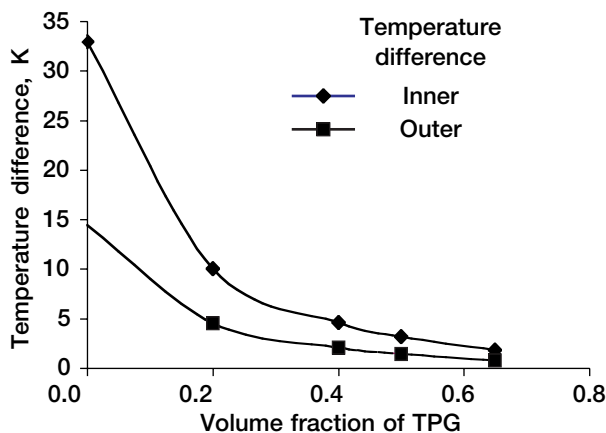Figure 7.—Total Al and TPG thickness and effective conductivity as functions of volume fraction of TPG.

Figure 8.—Temperature differences across inner and outer radiator sectors as functions of volume fraction of TPG.
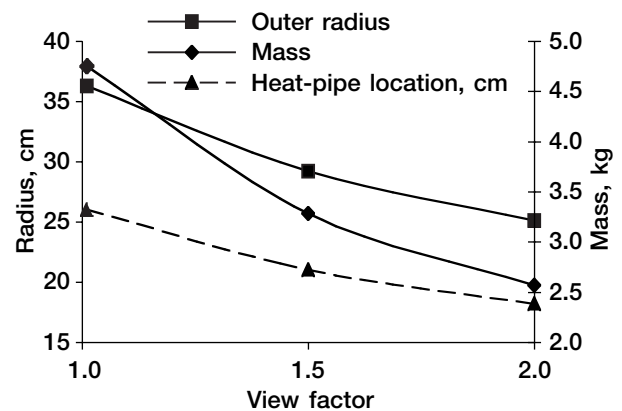

Figure 9.—Sensitivity of heat-pipe radiator mass, outer radius, and optimum heat-pipe location to view factor.
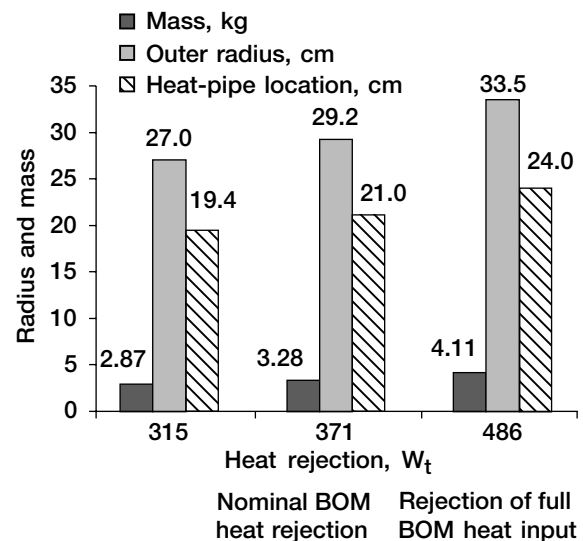

Figure 10.—Sensitivity of heat-pipe radiator mass, outer radius, and optimal heat-pipe location to heat rejection (at beginning of mission (BOM) near Earth, sink temperature, 205.8 K).

Heat-pipe radiator sensitivity results.—As explained in the previous section, the heat-pipe radiator reference parameters with a volume fraction of TPG = 0.4 were used as the reference case for a sensitivity study. Sensitivities of heat-pipe radiator mass, outer radius, and optimal radial heat-pipe location (hereinafter called the key radiator parameters) were determined for the following parameters: view factor to space, heat rejection, converter cold-end temperature, thermal conductivity, and radiator coating. These results are shown in figures 9 to 14.

Figure 9 shows the sensitivities of the key radiator parameters to the radiator view factor and shows the relative benefits of having unobstructed views on both sides of the radiator (view factor = 2). It is estimated that the best average view factor that can be hoped for with this Stirling power system application is in the range from 1.2 to 1.5. The radiator mass increases by about 1.5 kg (or about 45 percent) as the view factor is reduced from 1.5 to 1.0; the outer radius increases by about 25 percent for this same change in view factor.

Figure 10 shows the sensitivities of the key parameters to heat rejection. Waste heat rejection at BOM near Earth is expected to be about 371 W_t. If the radiator were sized to be able to reject the entire heat production of the GPHS heat source at BOM, it would have to reject 486 W_t. For the 54-percent increase in heat rejection from 315 to 486 W_t, the mass increases by 43 percent and the outer radius increases by 24 percent. The radiator temperature differences were not significantly affected by the range of heat rejection evaluated.

The sensitivities of the key parameters to the converter cold-end temperature are shown in figure 11. The radiator mass increases a little faster than linearly with decreases in the converter cold-end temperature. The mass increases by 1.3 kg (51 percent) as the temperature decreases from 423 to 377 K;
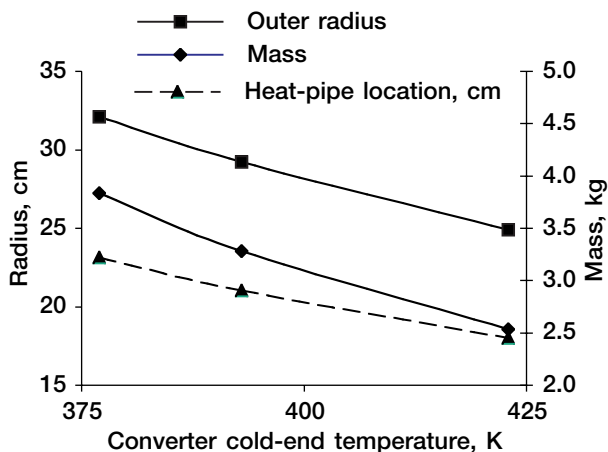
Figure 11.—Sensitivity of heat-pipe radiator mass, outer radius, and optimal heat-pipe location to converter cold-end temperature.
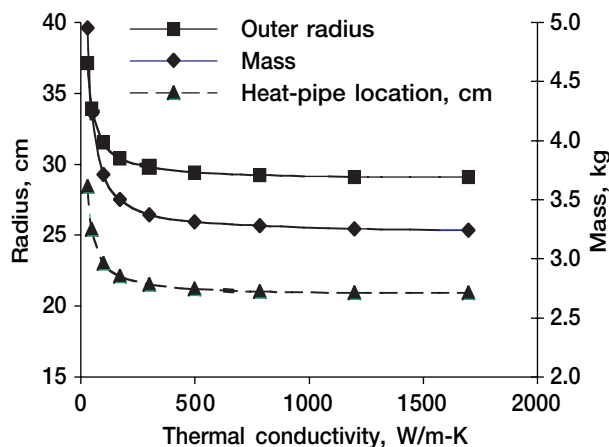

Figure 12.—Sensitivity of heat-pipe radiator mass, outer radius, and optimal heat-pipe location to thermal conductivity for fixed thickness (3.386 mm) and density (2.5 g/cm^3).
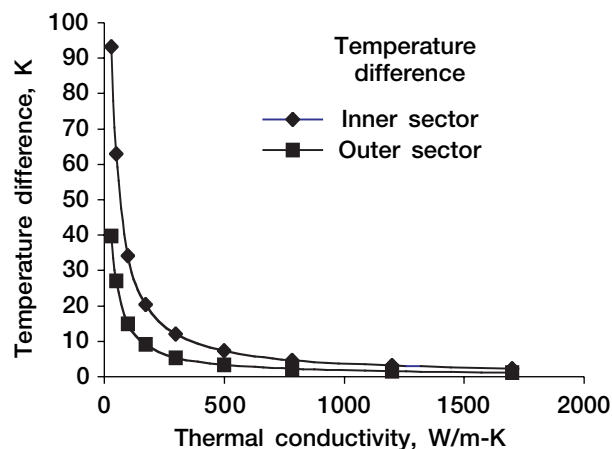

Figure 13.—Sensitivity of heat-pipe radiator temperature drop across inner and outer sectors to thermal conductivity for fixed thickness (3.386 mm) and density (2.5 gm/cm^3).

the outer radius increases by 7.2 cm, or 29 percent for the same decrease in the converter cold-end temperature. Again, radiator temperature differences were not significantly affected.

The assumptions used to determine sensitivities to thermal conductivity are as follows: total thickness and density were fixed at the reference values for the case of a TPG volume fraction of 0.40, 3.386 mm, and 2.52 g/cm^3, respectively. This thickness is the sum of the thickness of the two fins on each side of the heat-pipe/honeycomb sandwich. The reference composite thermal conductivity for the case of the TPG volume fraction of 0.40 was 784 W/m-K. The thermal conductivity was arbitrarily varied over a range from 30 to 1700 W/m-K (1700 W/m-K is the thermal conductivity of pure TPG in the plane of the fin). Sensitivities of the key radiator parameters to thermal conductivity are shown in figure 12. Note that for the given 3.386-mm thickness, the key parameters change very

little with thermal conductivity when the conductivity is greater than 500 W/m-K. For lesser thickness, such curves would likely flatten out at a higher value of thermal conductivity. For this same set of runs, the temperature differences across the inner and outer radiator sectors are shown in figure 13 as functions of thermal conductivity. The inner sector temperature difference is from the heat pipe to the inner radius; the outer sector temperature difference is from the heat pipe to the outer radius. For a conductivity greater than 500 W/m-K, the maximum temperature difference was about 7 K or less.

The sensitivities of the key parameters to three radiator coatings are shown in figure 14. The specifications of the first two coatings are as shown, whereas the third is an assumed ideal coating with an absorptivity of 0.0 and an emissivity of 1.0, which corresponds to a sink temperature of 3.0 K. The results for this ideal coating allow us to judge the relative merits of the two practical coatings, Z–93 and clear anodized Al, in approaching the capabilities of an ideal coating. The Z–93 and clear anodized Al radiators must be 8 percent and 31 percent more massive, respectively, than an ideally coated radiator to achieve the same heat rejection. Outer radii for these two practical coatings must be 5 percent and 18 percent greater, respectively, than those of an ideally coated radiator.

Carbon-carbon/TPG and beryllium/TPG fins.—Two additional runs were made with carbon-carbon and beryllium as the TPG encapsulants in place of aluminum. Carbon-carbon and beryllium both have a higher thermal conductivity than aluminum (350 and 220 W/m-K, respectively, versus 173 W/m-K) and lower densities (2.05 and 1.8 g/cm^3, respectively, versus 2.7 g/cm^3). Both additional runs were based on 0.40 volume fractions of TPG; therefore, the total fin thickness was the same (3.386 mm) for the Al/TPG, C-C/TPG, and Be/TPG runs. The key radiator parameters are compared for these TPG composite runs in figure 15. Outer radii and optimized heat-pipe locations for the three runs were identical.
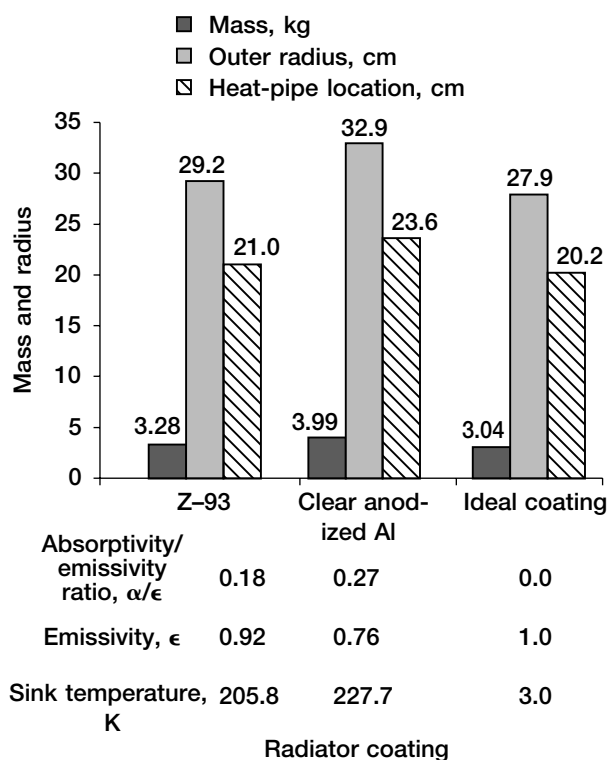
Figure 14.—Radiator mass, outer radius, and optimal heat-pipe location for Al/TPG (0.40-volume fraction TPG) radiator for three radiator coatings.

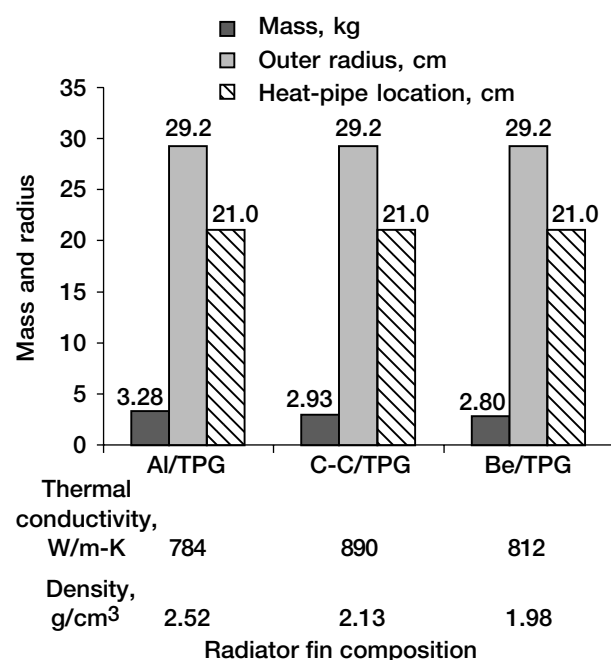| Radiator coating	Z–93	Clear anodized Al	Ideal coating
Absorptivity/emissivity ratio, α/ϵ	0.18	0.27	0.0
Emissivity, ϵ	0.92	0.76	1.0
Sink temperature, K	205.8	227.7	3.0

Figure 15.—Radiator mass, outer radius, and optimal heat-pipe location for three radiator fin compositions (Al, C-C, and Be combined with 0.40-volume fraction TPG); fixed thickness, 3.386 mm.

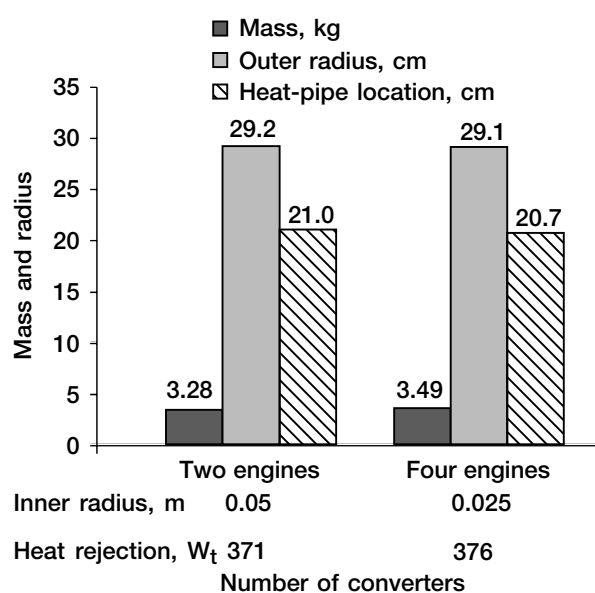| Radiator fin composition	Al/TPG	C-C/TPG	Be/TPG
Thermal conductivity, W/m-K	784	890	812
Density, g/cm^3	2.52	2.13	1.98

Figure 16.—Radiator mass, outer radius, and optimal heat-pipe location for Al/TPG (0.40-volume fraction TPG) radiator for two- and four-converter systems.

Number of converters	Two engines	Four engines
Inner radius, m	0.05	0.025
Heat rejection, W_t	371	376

Although a little surprising at first, a glance at the composite thermal conductivity for the three cases (shown at the bottom of the bar chart in figure 15) shows that they vary from 784 to 890 W/m-K. Figure 12 shows that for composite thermal conductivities greater than about 500 W/m-K, the key radiator parameters are very insensitive to further increases in the thermal conductivity. Therefore, the lower masses of the C-C/TPG and Be/TPG radiators (11 and 15 percent lower, respectively, compared with Al/TPG) are due to the lower densities of the C-C and Be relative to Al. The radiator temperature differences were less than 5 K for all cases.

Comparison of aluminum/TPG radiator designs for systems with two and four converters.—All the heat-pipe radiator runs discussed in previous sections were based on two Stirling converters with two 180° radiator sectors. For comparison, a run was made based on four Stirling converters with four 90° radiator sectors. Both the two- and four-converter systems were sized to produce the required 105 W_e 6 years after BOM. These results (for Al/TPG with 0.40 volume fraction of TPG) are compared in the bar chart of figure 16, which shows that the four-converter design is about 0.2 kg heavier because of the larger number of saddle interfaces (shown in fig. 3) required between the cold-end heat exchangers and the heat-pipe evaporators. It should be noted that the radiator inner radius for the four-converter system was 2.4 cm instead of the 5 cm for the two-converter layout. Also, heat rejection was 376 W_t for the four-converter case to account for a slightly reduced efficiency for the smaller converter. The rest of the heat-pipe radiator runs discussed next are for two converters and two 180° circular radiator sectors.
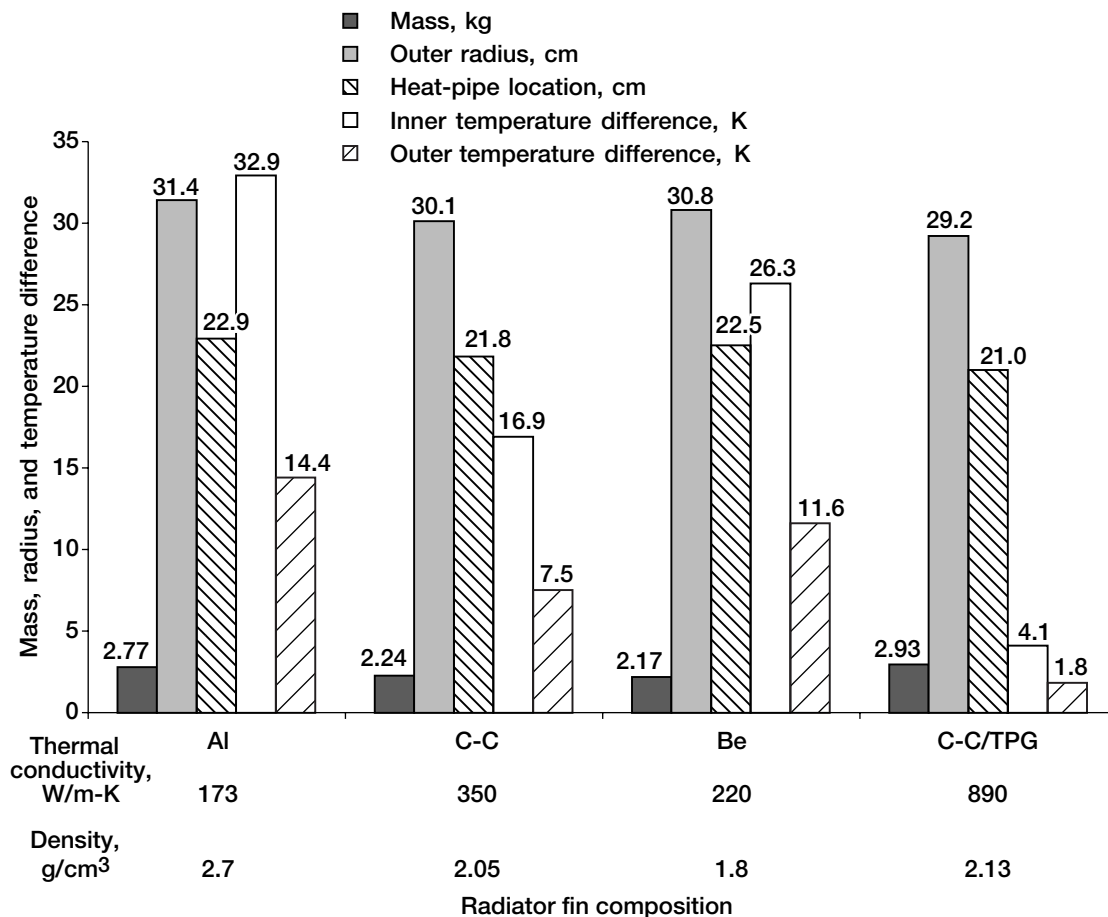
Figure 17.—Radiator mass, outer radius, and optimal heat-pipe location and inner and outer temperature differences for four radiator fin compositions (Al, C-C, and Be, 2.032 mm thick; C-C/TPG with 0.40-volume fraction TPG, 3.386 mm thick).

Pure aluminum, beryllium, and carbon-carbon fins.— Earlier it was shown that a radiator using pure Al fins (with an approx. 1-mm-thick fin on each side of the honeycomb, or a 2.032-mm Al thickness total, not including the honeycomb) was somewhat lighter than one with a 0.40-volume fraction TPG, Al/TPG fins but had a slightly larger outer radius. Since C-C and Be both have higher thermal conductivity and lower density than Al, design calculations were made for pure C-C and Be radiator fins (the honeycomb was still aluminum and the heat pipe and saddle were still copper). Comparisons of the design results for these radiators are shown in figure 17. Also shown for comparison is the previous design for the 0.40-volume fraction TPG, C-C/TPG. The radiators with Al, C-C, and Be fins all have a total fin thickness of 2.032 mm (total of the fins on each side of the honeycomb) and the C-C/TPG total fin thickness is 3.386 mm (both fins). Of the three pure component radiators, the C-C radiator is seen to have the smallest outer radius and heat-pipe radial location as a result of its higher thermal conductivity. The pure Be radiator has the least mass due to its smaller density. The significance of the larger heat-pipe radial location is that the copper heat pipe is

somewhat heavier. Note that the masses of the radiators with Al, C-C, and Be fins are all lighter than that with C-C/TPG fins; however, they are all somewhat larger in diameter and have greater temperature differences across the radiator.

Optimal versus fixed heat-pipe locations.—All the previous heat-pipe radiator runs were based on optimized heat-pipe locations to produce equal heat rejections in the radiator areas inward and outward of the heat-pipe radial location. For each of these runs, the heat-pipe location optimized at a greater radial location than the Stirling cold-end heat exchanger, which means that each heat pipe would need two bends to transition from the Stirling cold-end location to the optimized radial heat-pipe location. Another option is to fix the heat-pipe location at the radial location of the Stirling cold-end heat exchanger (14 cm from the radial center of the radiator fins for the converters considered in this study). Figure 18 shows the key radiator parameters for designs with optimized and fixed heat-pipe locations for radiators with Al, C-C, and Be fins. Figure 19 shows the temperature differences across the inner and outer radial sections for the same runs. For each of these radiator materials, figure 18 shows that fixing the heat-pipe location at
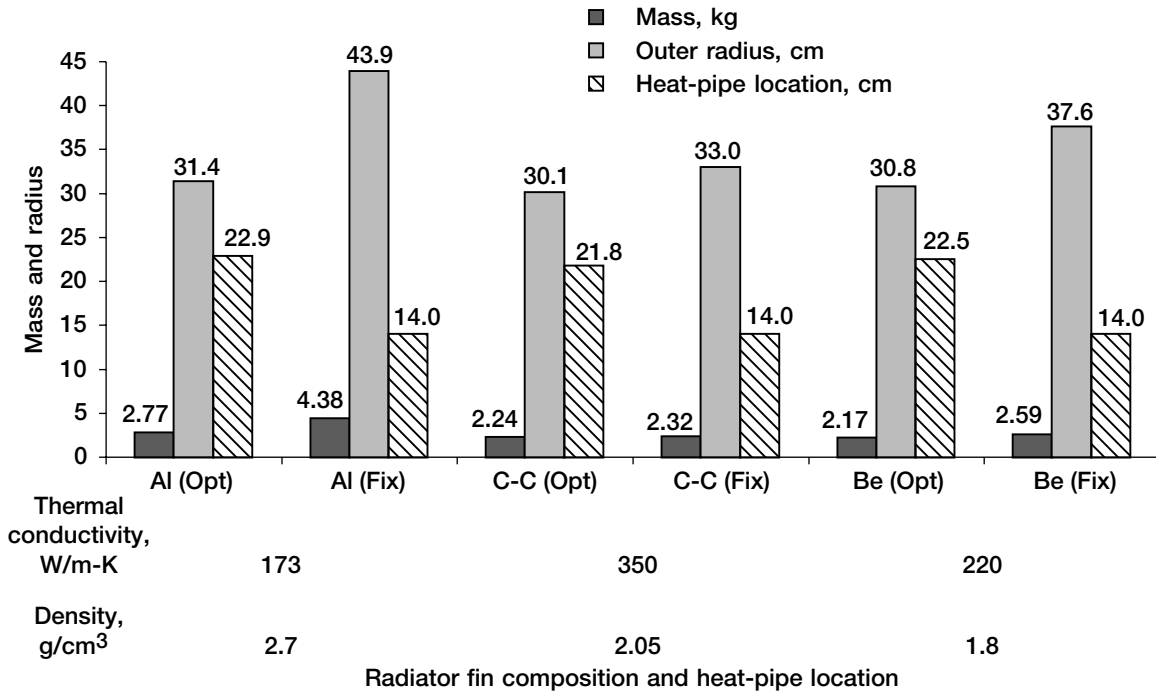
Figure 18.—Radiator mass, outer radius, and heat-pipe location for optimized and fixed heat-pipe locations for same fin thickness for Al, C-C, and Be.
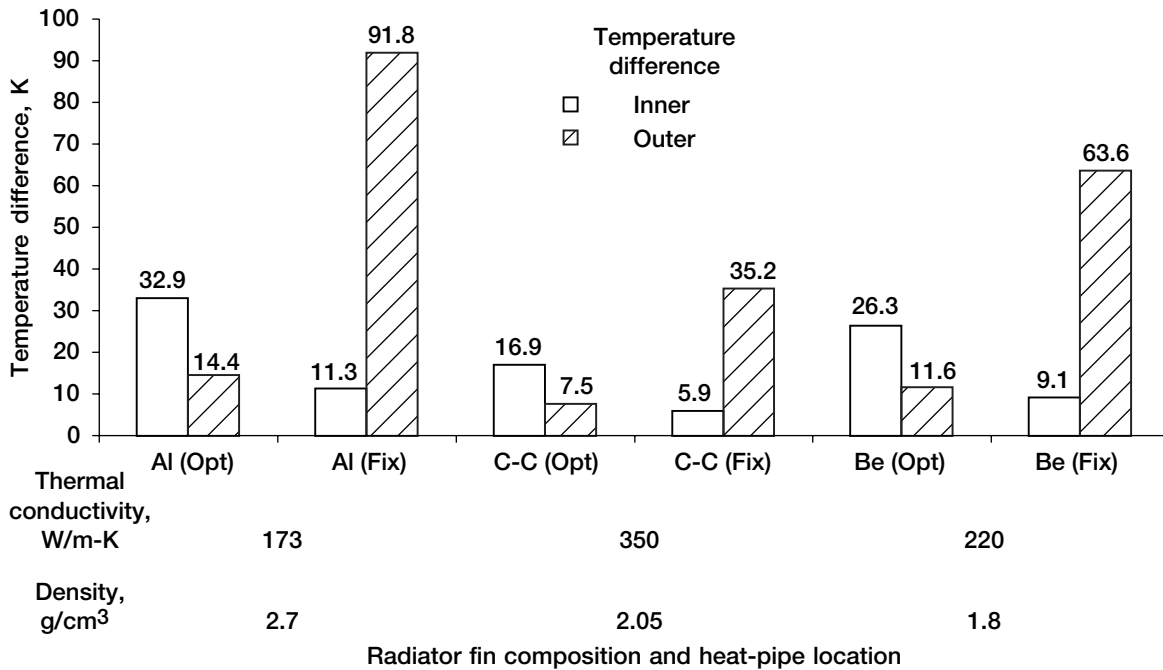

Figure 19.—Temperature differences across inner and outer sectors for optimized and fixed heat-pipe locations for same fin thickness for Al, C-C, and Be.

14 cm results in a larger outer radius. Figure 19 shows that for each of the fixed heat-pipe location designs, the maximum temperature drop is substantially larger than that for the corresponding optimized location design. It is also seen that the material with the largest thermal conductivity (C-C at k = 350 W/m-K) had the least increase in outer radius and maximum temperature difference, as might be expected. For each of the considered materials in figures 18 and 19, fixing the heat-pipe location also resulted in increased radiator mass; hence, for these cases, the increases in fin mass due to the larger outer radii outweigh the effect of smaller heat-pipe masses due to the smaller radii of the heat pipe.

Comparisons of optimized and fixed heat-pipe locations were also made for radiators with 0.40-volume fraction TPG, Al/TPG, and C-C/TPG fins. Comparisons of the key radiator parameters for these cases are shown in figure 20 and comparisons of temperature difference across the inner and outer sectors for the same runs are shown in figure 21. Figure 20 shows that fixing the heat-pipe location for these materials produces only small increases in the outer radius because of the large thermal conductivity of these composite materials (see values at bottom of fig. 20) as compared with those of the pure materials (Al, C-C, and Be). The relatively moderate increases in the maximum temperature differences in going from optimized to fixed heat-pipe location (fig. 21) are also due to the relatively large thermal conductivity of the composite materials. The masses actually decrease for the fixed heat-pipe location designs (fig. 20) because the increases in fin mass due to the slightly larger outer radii are outweighed by the decreases in heat-pipe mass attributed to the smaller heat-pipe radii.

No-Heat-Pipe Radiator Results

A conceptual design study was also conducted for no-heat-pipe radiators. For this concept, the inner radius of a single 360° circular radiator fin is in contact with the outer cylindrical surface of the Stirling cold-end heat exchanger (surface radius of 2.4 cm, fig. 5). Therefore, the plane of the fin is disk shaped with a concentric circular cutout for the converter. This concept has the advantage of eliminating the heat pipe and significantly reducing the temperature drop from the converter cold-end temperature to the radiator fin root temperature. For the heat-pipe radiator study, this temperature drop was assumed to be 15 K. It is estimated that the temperature drop across the contact surface between the converter cold end and the no-heat-pipe radiator should be no larger than 1 or 2 K. The reference temperature drop was assumed to be 2 K. A minimum average fin thickness of about 2 to 3 mm was assumed, based on the desire to maintain adequate stiffness for the radiator sizes anticipated. A number of materials, several fin shapes, and a range of thicknesses were studied. The mass quoted for each concept is a total radiator mass including all radiators in the system (two or four depending on the number of converters).

Sensitivities to radiator fin material, shape, and thickness.—Sensitivities of the key parameters, radiator mass, and outer radius were studied for various radiator fin materials, shapes, and thicknesses. Reference assumptions and/or parameters used for all the runs in this section were a BOM heat rejection of 371 W_t; radiator coating of Z–93 (α/ε of 0.18, ε of 0.92); an insolation angle of ±30°; and a minimum mission distance from the Sun of 0.9 AU, implying a sink temperature
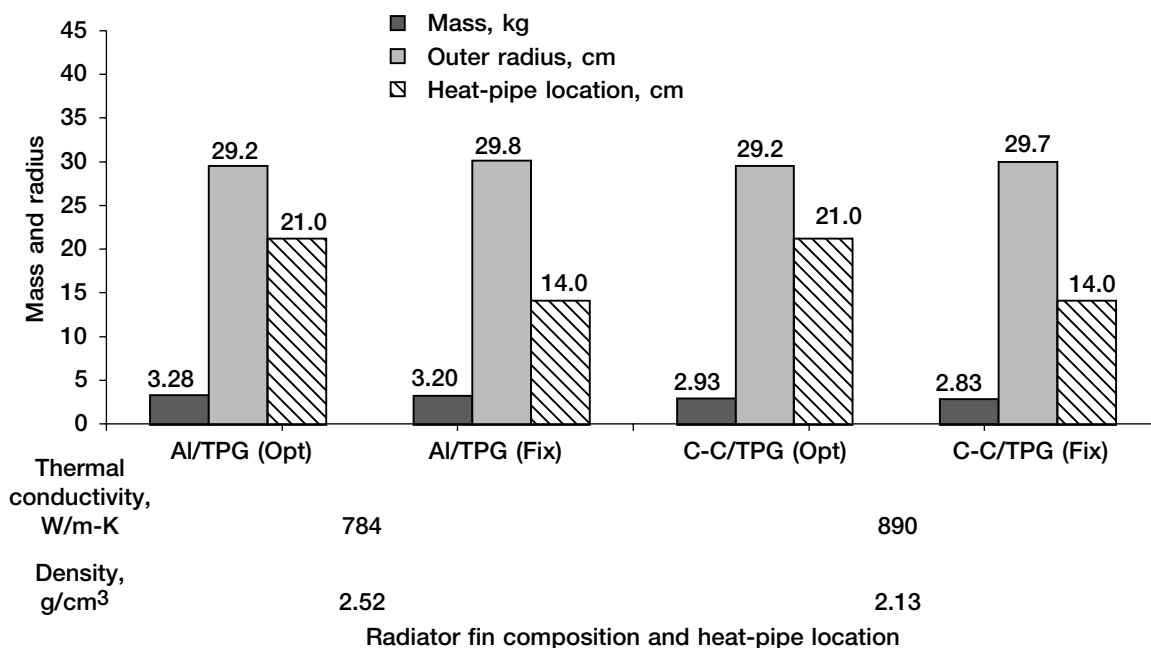

Figure 20.—Radiator mass, outer radius, and heat-pipe location for optimized and fixed heat-pipe locations for same fin thickness for Al/TPG and C-C/TPG with 0.40 volume fraction of TPG.
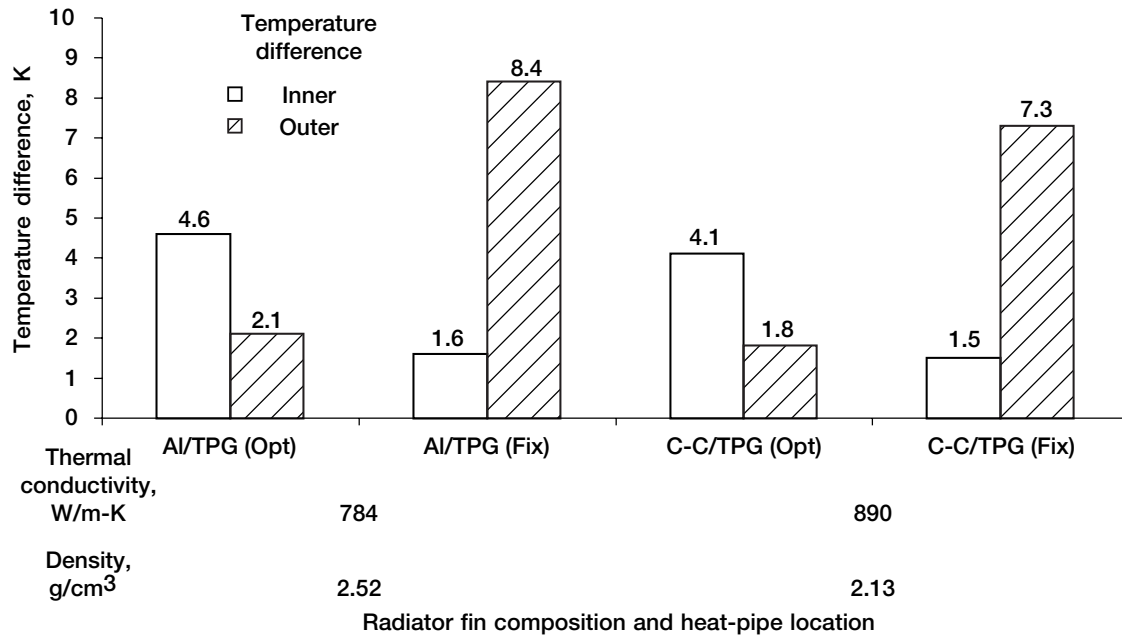
Figure 21.—Temperature differences across inner and outer sectors for optimized and fixed heat-pipe locations for same fin thickness for Al/TPG and C-C/TPG with 0.40 volume fraction of TPG.
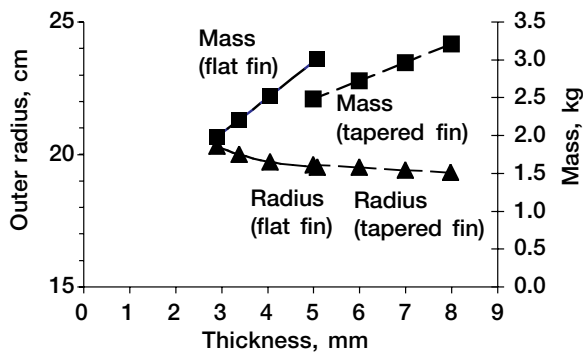

Figure 22.—No-heat-pipe radiator mass and outer radius as functions of Al/TPG flat fin thickness and Al/TPG tapered fin maximum thickness (taper is from max. thickness to 3 mm).
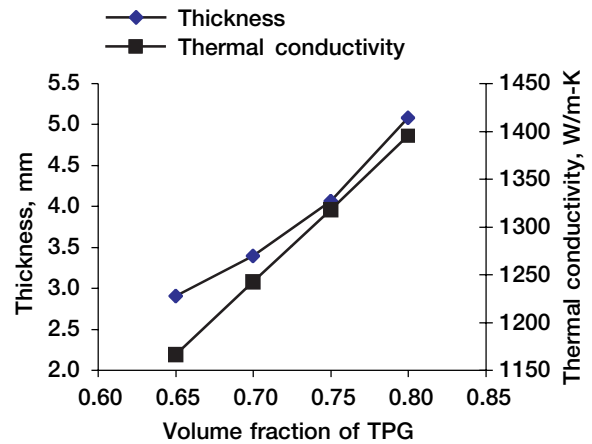

Figure 23.—Thickness and thermal conductivity of Al/TPG flat fin as functions of volume fraction of TPG.

of 205.8 K; a converter cold-end temperature of 393 K minus a 2 K drop, yielding a radiator fin root temperature of 391 K; an inner fin radius of 2.4 cm; and a radiator view factor to space of 1.5.

The key radiator parameter sensitivities to fin thickness for flat and tapered Al/TPG fins are shown in figure 22. The relations of the volume fraction of TPG for these fins to fin thickness and to composite thermal conductivity in the plane of the fin are shown in figure 23 for volume fractions of TPG from 0.65 to 0.80. For the tapered surfaces considered, the maximum thickness of the tapered fin is shown in the plots. The minimum thickness for each of the tapered fins was 3 mm. The minimum-mass tapered fin (5- to 3-mm taper) was 2.48 kg and had an outer radius of 19.6 cm. The minimum-mass flat fin (at 2.9 mm

thick corresponding to 0.65 volume fraction of TPG) was 1.98 kg and had an outer radius of 20.3 cm.

Similar sensitivity plots for Be/TPG fins are shown in figures 24 and 25. The minimum-mass tapered fin (5- to 3-mm taper) weighed 2.25 kg and had an outer radius of 19.6 cm. The minimum-mass flat fin (2.9 mm thick and having a 0.65 volume fraction of TPG) was 1.75 kg and had an outer radius of 20.2 cm. Sensitivity plots for C-C/TPG are shown in figures 26 and 27 for the minimum-mass tapered fin (5- to 3-mm taper) that was 2.3 kg and had an outer radius of 19.6 cm. The minimum-mass flat fin (also 2.9 mm thick and having a 0.65 volume fraction of TPG) was 1.81 kg and had an outer radius of 20.2 cm.
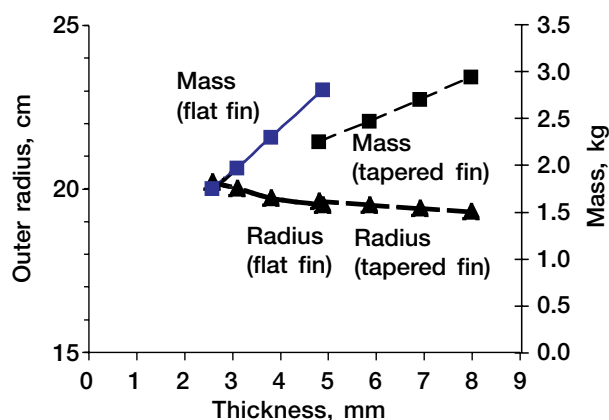
Figure 24.—No-heat-pipe radiator mass and outer radius as functions of Be/TPG flat fin thickness and Be/TPG tapered fin maximum thickness (taper is from max. thickness to 3 mm).

Figure 26.—No-heat-pipe radiator mass and outer radius as functions of C-C/TPG flat fin thickness and C-C/TPG tapered fin maximum thickness (taper is from max. thickness to 3 mm).

Figure 25.—Thickness and thermal conductivity of Be/TPG flat fin as functions of volume fraction of TPG.
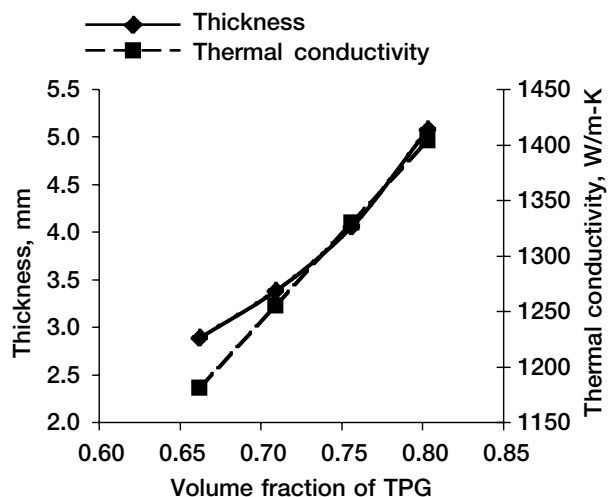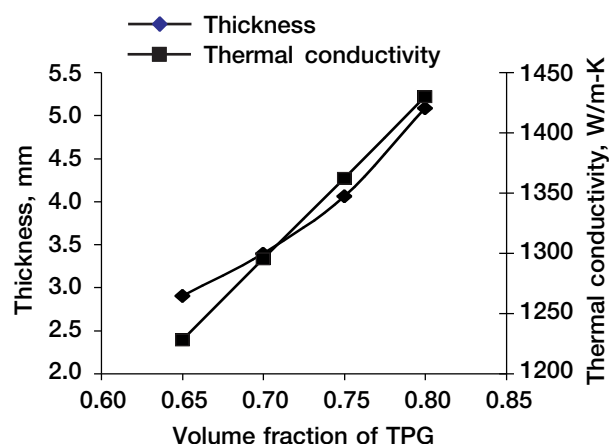

Figure 27.—Thickness and thermal conductivity of C-C/TPG flat fin as functions of volume fraction of TPG.

The outer radii are about the same for all three TPG composites because the composite thermal conductivity does not differ greatly for any of the composites (they are all dominated by the high thermal conductivity of TPG). The minimum masses for the three composites are also similar, ranging from 1.75 kg for Be/TPG to 1.98 kg for Al/TPG.

A similar sensitivity study was done for pure Al fins, and the results are shown in figure 28. Both tapered fins and fins with a parabolic surface were considered (since both should be practical for a pure metal). Flat fins were heavier than tapered and parabolic fins and are not shown. Plots are shown as functions of maximum thickness of the tapered and parabolic fins; the minimum thickness for both types of fins was 1 mm. The mass of the tapered fins minimized at a value of 4.64 kg at a thickness of 6 to 7 mm. The 7- to 1-mm tapered case was chosen as the best tapered configuration because it had the smaller outer radius of 25.7 cm; the maximum fin temperature

difference was 63 K. The parabolic fins have a smaller minimum mass of 4.01 kg, which occurred for a fin ranging in thickness from 8 to 1 mm with an outer radius of 27.4 cm; the maximum fin temperature difference was 76 K. The radius could be reduced a few centimeters to 25.2 cm and the maximum fin temperature difference could be reduced to 62 K by increasing the heat flow area for a small 0.12-kg mass penalty.

Similar results are shown for pure Be fins in figure 29. Again, flat fins were heavier than tapered and parabolic fins and are not shown. For the tapered fins, the minimum mass was 2.57 kg for a taper ranging from 5 to 1 mm with an outer radius of 26.5 cm; the maximum fin temperature difference was 68 K. For the parabolic fins, the minimum mass was 2.20 kg for a thickness varying from 6 to 1 mm with an outer radius of 27.6 cm; the maximum fin temperature difference was 76 K. For the parabolic fin, the outer radius could be reduced to 23.4 cm and the maximum fin temperature difference to 48 K for a mass penalty of 0.26 kg.

Figure 28.—No-heat-pipe radiator mass and outer radius as functions of Al tapered fin and parabolic fin maximum thickness (taper, or parabola, is from max. thickness to 1 mm).

Figure 29.—No-heat-pipe radiator mass and outer radius as functions of Be tapered fin and parabolic fin maximum thickness (taper, or parabola, is from max. thickness to 1 mm).
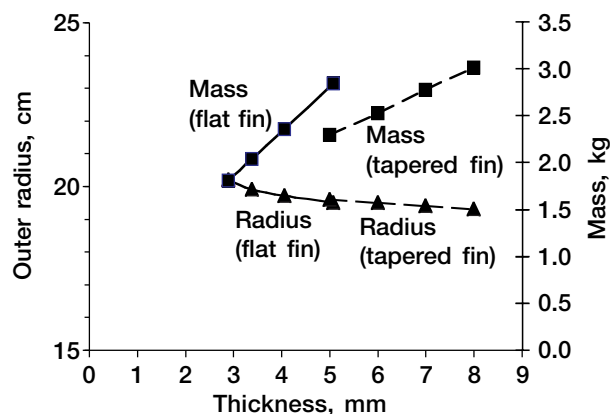

Figure 30.—No-heat-pipe radiator mass and outer radius as functions of C-C flat fin thickness and tapered fin maximum thickness (taper is from max. thickness to 2 mm).
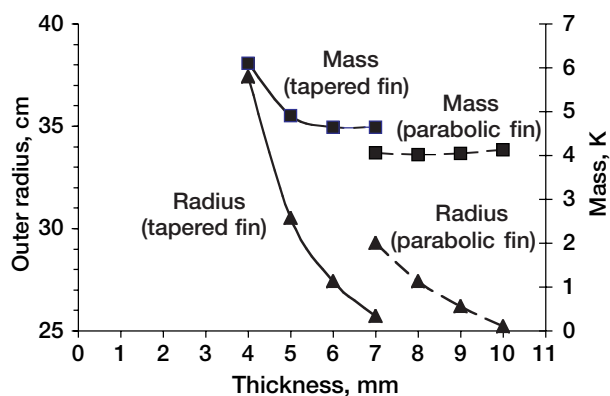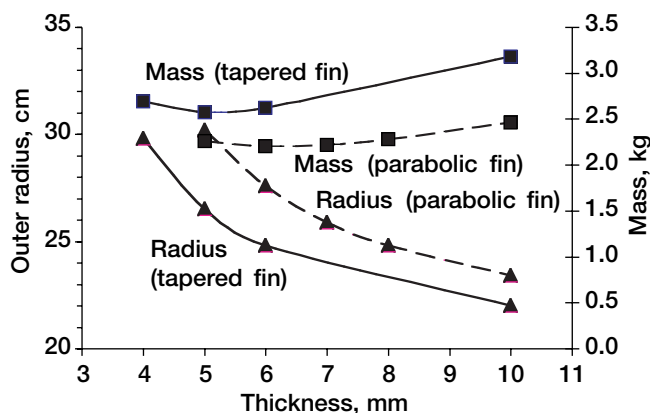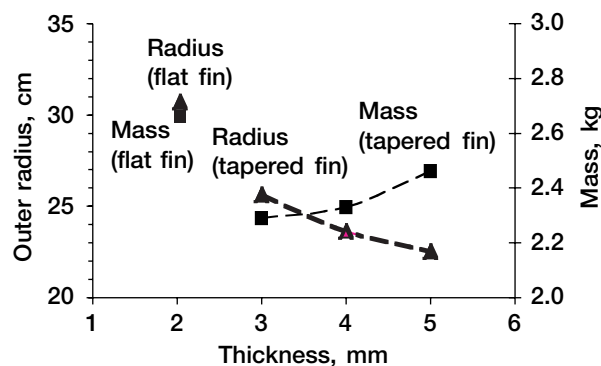
Results are shown for C-C fins in figure 30. One flat fin case is shown for a thickness of about 2 mm. The radiator mass was 2.66 kg and the outer radius was 30.7 cm; the maximum fin temperature difference was 86 K. The tapered fin cases varied from the maximum thickness shown in figure 30 down to 2 mm; a thickness less than 2 mm was assumed impractical for C-C for this concept. The minimum mass was 2.29 kg for a taper from 3 to 2 mm and an outer radius of 25.6 cm; the maximum fin temperature difference was 59 K. For the tapered fin, the outer radius could be reduced to 22.5 cm and the maximum fin temperature difference reduced to 37 K for a mass penalty of 0.17 kg.

Maximum fin temperature differences for the minimum-mass case for each material are shown in figure 31 and are about 14 to 15 K for each. The maximum temperature differences decrease with increasing TPG volume fraction. The results of the above sensitivity to material, shape of fins, and thickness are all summarized in figures 31 and 32 where the minimum-mass cases for each of the different materials are compared. All

TPG designs have a significantly smaller mass, outer radius, and maximum temperature difference than designs with the pure materials. The flat, 2.9-mm-thick Be/TPG fin had the least mass of 1.75 kg and equaled the smallest radius of 20.2 cm. The C-C/TPG and Al/TPG fins were only slightly heavier than the Be/TPG fins and had essentially the same outer radius and maximum temperature difference. Of the designs with pure Al, C-C, and Be fins, Be made possible the lightest radiator of the three. However, the C-C design was only slightly heavier and had a smaller outer radius than the Be radiator fin. The pure Al fin was 75 percent heavier than the C-C fin.

In figure 31, note the large temperature differences across the pure material fins. The large temperature differences as compared with those for the TPG composites are related to the much lower thermal conductivity of the pure materials (material thermal conductivity is compared in fig. 32). The large pure material temperature drops suggest that these designs will be much more sensitive to any variabilities in the hardware fabrication processes; therefore, fin section thickness (and mass) may need to be increased to reduce temperature differences and thus ensure achieving the desired design performance. This is especially true for radiator coatings such as Z–93, which may degrade if temperature differences across the radiator exceed several tens of degrees kelvin.

Comparison of aluminum and beryllium radiator designs for systems with two and four converters.—No-heat-pipe radiator designs for two- and four-converter systems are compared in figure 33. Heat rejected for the two cases was slightly different because of small assumed differences in converter efficiency (converters for the two-converter system are larger and slightly more efficient). For the two-converter case, heat rejection was 371 W_t and for the four-converter case, 376 W_t.

However, it should be remembered that the heat load for each radiator of a four-converter power system is approximately half that for a two-converter system. As a result, the four-converter system shows some mass and performance gains.

Figure 33 shows that for the parabolic (8- to 1-mm) Al design, changing from a two- to a four-converter system layout
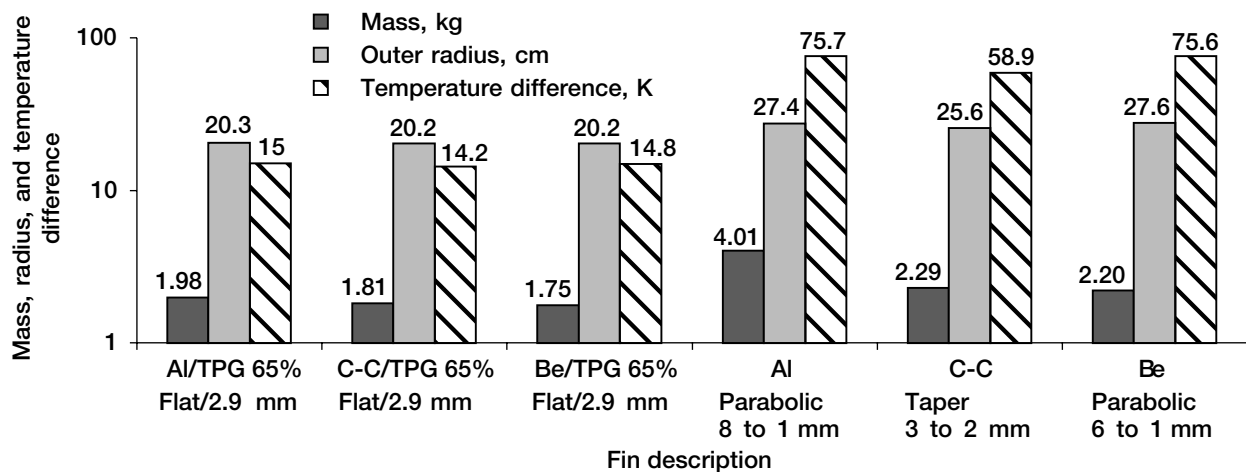
Figure 31.—Comparison of least-mass cases for no-heat-pipe radiators with Al/TPG, C-C/TPG, Be/TPG, Al, C-C, and Be fins. Mass, outer radius, and temperature difference across the radiator fins shown for each case.
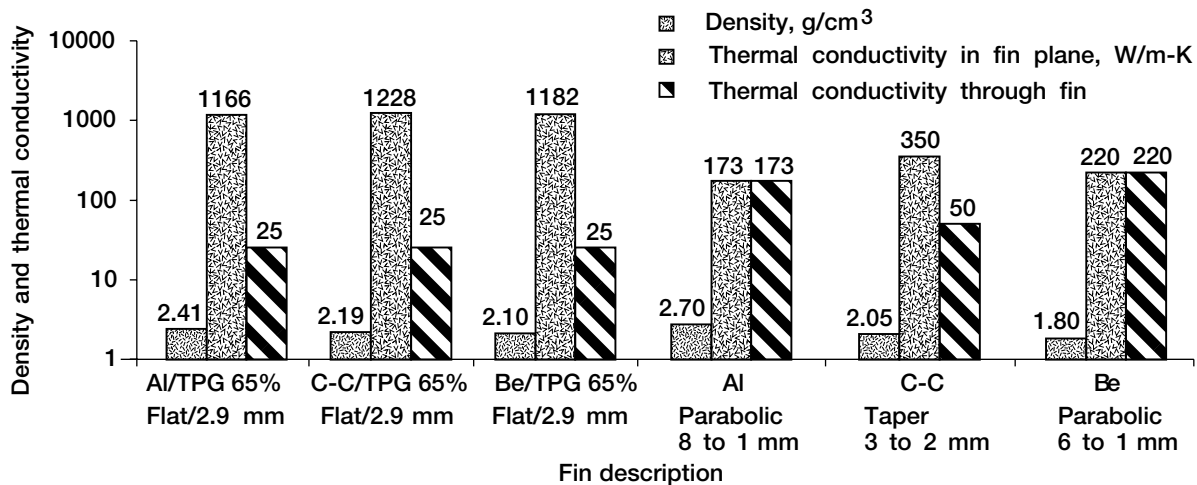
Figure 32.—Radiator properties for least-mass cases for no-heat-pipe radiators with Al/TPG, C-C/TPG, Be/TPG, Al, C-C, and Be fins. Density and thermal conductivities in the plane of the fin and through the fin shown for each case.

reduces the radiator mass from 4.01 to 2.70 kg, the outer radius from 27.4 to 15.2 cm, and the temperature difference across the radiator fin from 76 to 29 K. For the Be parabolic (6- to 1-mm) design, the same change reduces the radiator mass from 2.2 to 1.6 kg, the outer radius from 27.6 to 15.2 cm, and the temperature difference from 76 to 29 K. Note that this figure also shows little difference in the outer radii and temperature differences for the corresponding Al and Be designs because their thermal transport capabilities are similar.

As mentioned above, for the Al and Be disk radiator designs, there appear to be major advantages in reduced radiator mass and temperature difference due to the reduced radiator size for the four-converter case. However, one major question related to this radiator comparison deals with the view factor that was

left equal to 1.5 for both two- and four-converter cases. In actuality, the radiators for the four-converter case might have substantially smaller view factors than that for the two-converter case. It would require a careful analysis of each system's geometry and its effect on the view factors for each radiator to accurately determine this temperature difference.

No-heat-pipe radiator sensitivity to view factor, heat rejection, converter cold-end temperature, and thermal conductivity.—The radiator design with a flat (0.65-volume fraction TPG) Al/TPG 360° disk fin was used for this sensitivity study. Sensitivities of the key radiator parameters, mass, outer radius, and temperature difference, were determined to view factor, heat rejection, converter cold-end temperature, and thermal conductivity. These results are shown in figures 34 to 39.
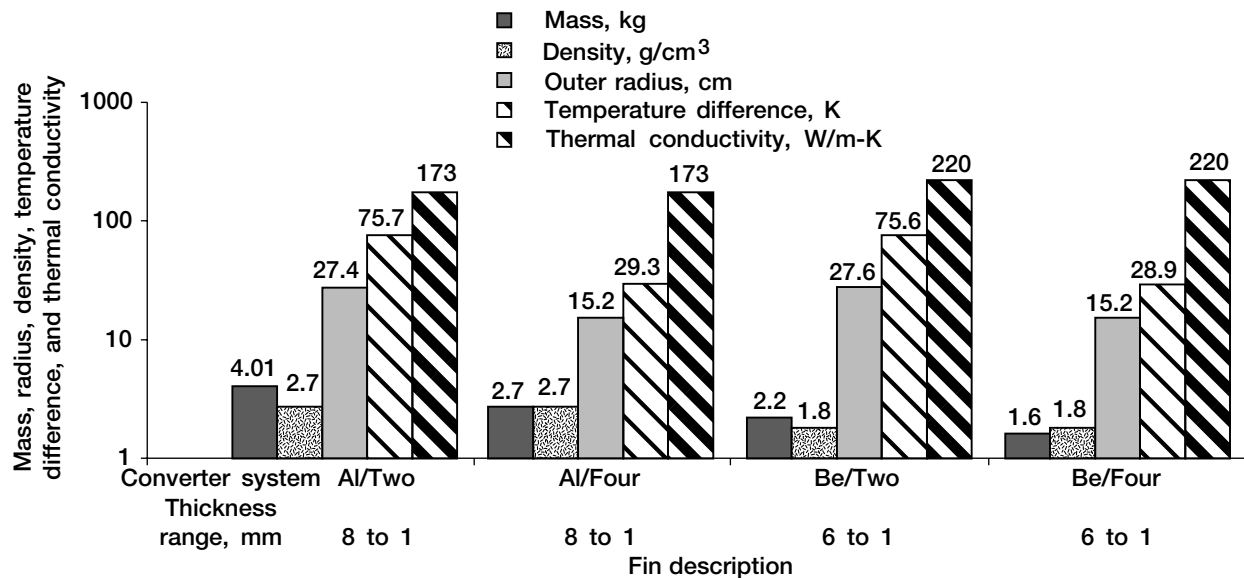
Figure 33.—Comparison of least-mass no-heat-pipe radiators for two- and four-converter system Al and Be parabolic fins. Mass, density, outer radius, temperature difference, and thermal conductivity across the radiator shown for each case.
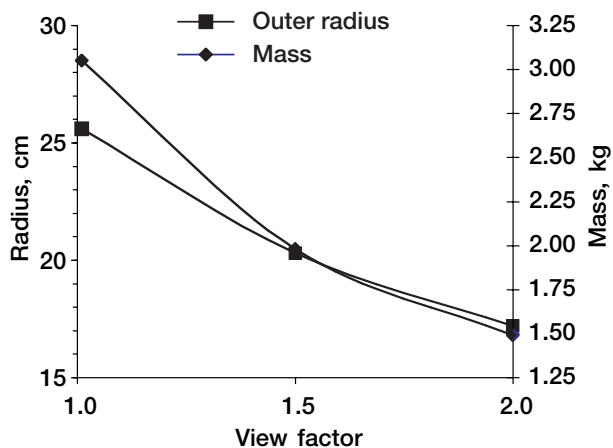
Figure 34.—Sensitivity of no-heat-pipe radiator mass and outer radius to view factor for flat (0.65-volume fraction TPG) Al/TPG.

Figure 35.—Sensitivity of temperature difference from inner to outer radius and sink temperature to view factor for flat (0.65-volume fraction TPG) Al/TPG.

Figure 34 shows the sensitivities of the key radiator parameters to radiator view factor and the relative benefits of having unobstructed views on both sides of the radiator (view factor = 2). Again, it is estimated that the best average view factor that can be expected for this Stirling power system application is in the range from 1.2 to 1.5. The radiator mass increases by 1.1 kg (or about 54 percent) as the view factor is reduced from 1.5 to 1.0, and the outer radius increases by 26 percent. Figure 35 shows the sensitivity of temperature difference across the radiator and the sensitivity of sink temperature to view factor for these same designs.

Figure 36 shows the sensitivities of the key parameters to heat rejection. For the 54-percent increase in heat rejection from 315 to 486 W_t, the mass increases by 62 percent, the outer radius increases by 30 percent, and the temperature difference increases by 80 percent. Sensitivities of the key parameters to converter cold-end temperature are shown in figure 37. The radiator mass increases by 0.9 kg (63 percent) as the temperature decreases from 423 to 377 K. The outer radius increases by 5.3 cm (31 percent) and the temperature difference increases by 2.5 K for the same change in converter cold-end temperature.
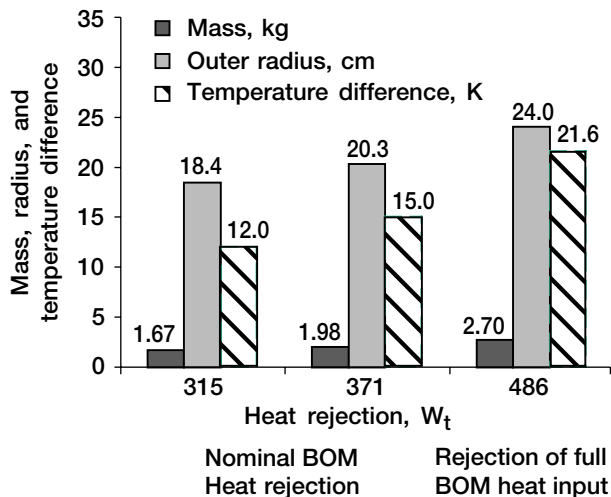
Figure 36.—Sensitivity of no-heat-pipe radiator mass, outer radius, and temperature difference to heat rejection for flat (0.65-volume fraction TPG) Al/TPG.

Figure 38.—Sensitivity of no-heat-pipe radiator mass, outer radius to thermal conductivity for fixed thickness and density (2.41 g/cm^3) for flat (0.65-volume fraction TPG) Al/TPG.

Figure 37.—Sensitivity of no-heat-pipe radiator mass, outer radius, and temperature difference to converter cold-end temperature for flat (0.65-volume fraction TPG) Al/TPG.
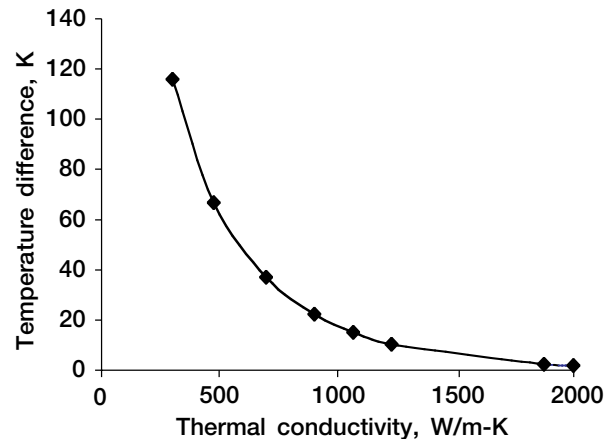
Figure 39.—Sensitivity of radiator temperature difference from inner to outer radius to thermal conductivity for fixed thickness (2.903 mm) and density (2.41 gm/cm^3) for flat (0.65-volume fraction TPG) Al/TPG.

The sensitivities to thermal conductivity are shown in figures 38 and 39. The following assumptions were used to determine these sensitivities: total thickness and density were fixed at the reference values for the 0.65-volume fraction Al/TPG case, 2.903 mm and 2.41 g/cm^3, respectively; the reference composite thermal conductivity for the 0.65-volume fraction Al/TPG was 1166 W/m-K; and the thermal conductivity was varied over a range from 200 to 10 000 W/m-K (1700 W/m-K is the thermal conductivity of pure TPG in the plane of the fin). The sensitivities of mass and outer radius are shown in figure 38. Note that for the given 2.903-mm thickness, these key parameters changed very little once the thermal conductivity became greater than about 1000 W/m-K. For this same set of runs, the sensitivity of the temperature difference from the inner to the outer radius is shown in figure 39. For the given 2.903-mm thickness, the thermal conductivity must be above 1700 W/m-K to reduce the temperature difference to less than 10 K. For the heat-pipe radiator runs (see fig. 13), the thermal conductivity had to be greater than 500 W/m-K to reduce the maximum temperature difference to less than 7 K for the larger 3.386-mm thickness. However, it should be remembered that for the no-heat-pipe radiator, the temperature drop is from the fin root temperature at the inner radius to the outer radius. For the heat-pipe radiator, the temperature drop is from the fin root temperature at the heat pipe (located between the inner and outer radii) to the inner radius and the outer radius.

Comparison of Heat-Pipe and No-Heat-Pipe Radiator Results

The three cases of least-mass heat-pipe and no-heat-pipe radiator designs are compared in table I. In the description column, for example, C-C/TPG40 designates a heat-pipe radiator design with fins that are a composite of carbon-carbon (which is a composite itself) and a 0.40 volume fraction of TPG. The fixed heat-pipe designs consist of a heat-pipe location fixed at the same radial location as the Stirling cold-end heat exchanger. The last design is the no heat pipe. Table I shows the key parameters of mass, outer radius, and maximum temperature difference. These results are referred to in the comparisons discussed next.

Before comparing the best heat-pipe and no-heat-pipe designs, several other considerations relative to the various materials under consideration should be mentioned. Although Be has certain health hazards associated with its dust and must be handled properly, solid machining of Be and using liquid coolants to wash away the chips is accomplished regularly today. Carbon-carbon is just beginning to be used for space radiators and there may be questions relative to joining it and coating it with a low-absorptivity/emissivity coating such as Z–93. Joining issues and mismatches (of the coefficient of thermal expansion) must be considered for all designs. Thermal pyrolytic graphite with its various encapsulants is just being developed. Aluminum/TPG is the most available current combination. Some parts have also been made of C-C/TPG, but due to the higher cost of beryllium, Be/TPG panels have not yet been fabricated in quantity. However, a relatively new aluminum-beryllium alloy referred to as "AlBeMet" has thermal and physical properties very close to those of beryllium. Hence, it may be an excellent encapsulant for TPG.

For the heat-pipe radiators with the heat pipe located at the optimal position, the designs with pure material fins (Al, C-C, and Be) appear to be a good choice. They are lighter than the designs with the TPG composite fins although they are slightly larger and have greater temperature differences. Of these, the C-C and Be designs are the lightest and smallest. However, the heat-pipe radiator with Al fins is only 0.5 to 0.6 kg heavier and has an outer radius only 0.6 to 1.3 cm larger and thus may be acceptable. The Al fin maximum temperature difference is the largest at 33 K.

The heat-pipe radiator designs with the TPG fins illustrate the effectiveness of the high TPG thermal conductivity in reducing the maximum temperature difference. For these designs, the maximum temperature difference is only 4 to 5 K. Note that the TPG fins are almost twice as thick as those for the non-TPG designs. The minimum thickness limitations on the encapsulant (for strength) and the TPG (for fabrication purposes) tend to make the TPG fins thicker. The heat-pipe radiator fin thickness is the total thickness of the two fins located on either side of the aluminum honeycomb-heat-pipe structure. The requirement of using two relatively thick flat TPG fins for

the heat-pipe concept apparently eliminates any mass benefit of using this high-conductivity composite.

The tradeoffs change for the heat-pipe radiators when the requirement is that the heat pipe be located at the same radial location as the Stirling cold-end heat exchanger. These comparisons are shown in the category "Fixed heat-pipe location" in table I. The heat-pipe radiators with pure Al and Be are significantly larger in size and have much larger temperature differences (and mass for Al). The heat-pipe radiators with TPG fins appear to be the better choice with their small size and temperature difference and reasonable mass. The pure C-C fins may be an acceptable alternative to the TPG fins.

For the no-heat-pipe designs, the flat TPG fins (Al/TPG, C-C/TPG, and Be/TPG) have definite advantages. They are all lighter and significantly smaller and have much lower temperature differences than the pure-material fins, even though the pure-material fin designs used tapered and parabolic surfaces to reduce mass. The Al/TPG fin design was only slightly heavier than those with the Be/TPG or C-C/TPG fins and may be the preferred choice because of its more advanced state of development. The C-C tapered fins and parabolic Be fins are only about 0.4 to 0.55 kg heavier than the TPG no-heat-pipe designs. Also, their size, although significantly larger than the sizes of the TPG designs, is still smaller than those for the heat-pipe radiators. The temperature differences of 60 to 75 K are rather large.

Both the temperature difference and size could be reduced by increasing the thickness (and mass), as illustrated by the two Be reduced-temperature-difference runs shown near the bottom of table I (described as Be reduced DT#1 and #2). Increasing the maximum thickness of the no-heat-pipe Be parabolic fin from 6 to 10 mm reduced the temperature difference from 75.6 to 47.5 K and the outer radius from 27.6 to 23.4 cm while the mass increased from 2.20 to 2.46 kg. The no-heat-pipe reduced DT#2 run shows that further reductions in temperature difference (to 34.3 K) and outer radius (to 22.0 cm) can be achieved at the cost of further increases in mass (to 3.18 kg) if a tapered (10- to 1-mm) Be fin is used instead of a parabolic (10- to 1-mm) Be fin.

It is clear from table I that the better no-heat-pipe radiator designs are lighter and have outer radii that are two-thirds as large as the better heat-pipe designs. However, the best designs require the use of TPG fins and also the power system to be mounted farther from the spacecraft because of the orientation of the radiator. It should be remembered that a view factor of 1.5 was used for all the designs in table I. Since the no-heat-pipe radiators will be facing each other across the GPHS heat source, these designs may have a smaller view factor than the heat-pipe radiator designs (although one side of the heat-pipe radiator will probably be facing the spacecraft, which may offset much of this difference). All designs will need to be iteratively reevaluated to arrive at final power system and spacecraft layouts on the basis of view factors determined by ray-tracing techniques. Note that because of their size in the

orthogonal plane, the no-heat-pipe radiators may also require a cutout to allow the mechanical connection of the two opposed converters necessary to minimize vibration. The reduced reliability of the heat-pipe designs is also a consideration in making a final decision between the two concepts.

Table II shows the breakdown of radiator mass into its several components for both heat-pipe and no-heat-pipe designs. The designs listed in table I are also given in table II with the exception of the two reduced-temperature-difference Be designs and three four-converter designs that were reported in earlier sections of the results. The heat-pipe radiator mass consists of fin, heat pipe (Cu), honeycomb (Al), and saddle (Cu) masses. The four-converter, optimized-heat-pipe-location Al/TPG40 design saddle mass is increased to roughly account for more but smaller saddles. The no-heat-pipe radiator mass consists of the fin and collar masses. The mass of each collar was estimated to be 0.1 kg per converter for both the two- and four-converter designs.

Summary of Results

The finite-difference code GPHRAD (General Purpose Heat (Source Power System) Radiator) and the space sink temperature calculation code TSCALC were developed at the NASA Glenn Research Center for the purpose of analyzing and designing circular sector radiators for Stirling radioisotope space power systems for NASA deep space missions. These codes were used to evaluate heat-pipe and no-heat-pipe radiator conceptual designs using a variety of standard and advanced materials. Designs with an optimal heat-pipe location were compared with designs with the heat pipe at the same radial location as the Stirling cold-end heat exchanger. A nominal system power output of 105 W_e was required 6 years after the beginning of the mission (BOM). The nominal heat rejection from the radiators used in the study was 371 W_t. The major results of this study follow.

Heat-Pipe Radiator Designs

1. The heat-pipe radiator layout chosen was a square 2-cm cross-section heat pipe embedded in an aluminum (Al) honeycomb with high-thermal-conductivity, circular-sector-panel fins attached on either side of the honeycomb. A heat pipe embedded directly in a tapered thermal pyrolitic graphite (TPG) fin may be appropriate for lower values of rejected heat and for heat pipes of no more than about 6-mm thickness.

2. Aluminum (Al), beryllium (Be), and carbon-carbon (C-C) were evaluated as encapsulant materials for the very high-conductivity TPG (1700 W/m-K in two orthogonal directions and 25 W/m-K in the third direction). For a 0.5-mm Al encapsulant thickness and a 0.40 volume fraction of TPG, the composite thermal conductivity for the Al/TPG fin was 784 W/m-K. A 0.5-mm C-C encapsulant with a 0.40 volume fraction of

TPG gave the highest composite thermal conductivity of 890 W/m-K. A 0.5-mm Be encapsulant with a 0.40 volume fraction of TPG had the lowest composite density of 1.98 g/cm^3.

3. For the 0.40-volume fraction TPG and optimized heat-pipe locations, Al/TPG, C-C/TPG, and Be/TPG fins all gave the same radiator outer radius of 29.2 cm. The total radiator mass was slightly lower with Be/TPG at 2.80 kg versus 2.93 kg for C-C/TPG and 3.28 kg for Al/TPG. The maximum temperature difference for all TPG designs was only 4 to 5 K.

4. Pure Al, Be, and C-C fins were also investigated and gave good results for designs with optimized heat-pipe locations. The least-mass designs for these fins have total radiator masses that were lower than those for the TPG designs, varying from 2.17 kg for Be fins to 2.77 kg for Al fins. This difference was due to the assumed TPG fabrication constraints for these sizes of radiators requiring a greater thickness for the TPG compared with that required for the pure materials. However, using the pure materials, the radiator size was somewhat greater, varying from 30.1 cm for C-C to 31.4 cm for Al, and the maximum temperature differences were also larger, varying from 17 K for C-C to 33 K for Al.

5. Fixing the heat-pipe location at the same radius as the Stirling cold-end heat exchanger would eliminate two 90° bends in the fabrication of each heat pipe. With this constraint, the C-C/TPG and Al/TPG fins resulted in much smaller radiators: a 29.7-cm outer radius for C-C/TPG and a 29.8-cm outer radius for Al/TPG compared with a 33.0-cm outer radius for C-C fins, a 37.6-cm outer radius for Be fins, and a 43.9-cm outer radius for Al fins. The maximum temperature differences were also much smaller: 7 to 8 K for the TPG cases compared with 35 K for C-C, 64 K for Be, and 92 K for Al. Designs with C-C (2.32 kg) and Be (2.59 kg) were still the lightest compared with 2.83 kg for C-C/TPG and 3.20 kg for Al/TPG. However, Al fins now gave the heaviest design at 4.38 kg. Both size and temperature difference for the C-C and Be fins could be reduced by increasing the fin thickness and mass.

6. Sensitivities to view factor, heat rejection, and converter cold-end temperature were determined for a radiator design with a 0.40 volume fraction of TPG, Al/TPG fins, and optimal heat-pipe location. Each significantly influenced the radiator size and mass. For this study, view factor was the least known of these parameters. For a range of view factors from 1 to 2, the total radiator mass varied from 4.75 to 2.57 kg and the outer radius varied from 36.3 to 25.1 cm.

7. The Z–93 and clear anodized Al surface coatings were compared for a radiator design with 0.40-volume fraction TPG, Al/TPG fins. The Z–93 coating has an absorptivity/emissivity ratio α/ε of 0.18 with an ε of 0.92, whereas clear anodized Al has an α/ε of 0.27 with an ε of 0.76. The Z–93 gave a total radiator mass of 3.28 kg and an outer radius of 29.2 cm compared with 3.99 kg and 32.9 cm for clear anodized Al.

8. For a fixed fin thickness (3.386 mm for both fins) and density, the thermal conductivity was arbitrarily varied over a

TABLE II.—BREAKDOWN OF RADIATOR MASS FOR LEAST-MASS HEAT-PIPE AND NO-HEAT-PIPE
DESIGNS FOR VARIOUS MATERIALS

[Coating, Z–93 (absorptivity/emissivity ratio α/ε, 0.18 where ε = 0.92); view factor to space F, 1.5; distance from Sun,
0.9 AU; reference sink temperature, 205.8 K; converter cold-end temperature, 393 K; fin root temperature for
heat-pipe case, 393 – 15 K = 378 K, and for no-heat-pipe case, 393–2 K = 391 K; heat rejection for
two-converter case, 37/W_t, and for four-converter case, 376 W_t.]

Description	Mass, kg					
	Fin	Heat pipe	Honeycomb	Saddle	Collar	Total
Optimized heat-pipe locations						
Al	1.65	0.54	0.19	0.39		2.77
C-C	1.16	0.51	0.18	0.39		2.24
Be	1.06	0.53	0.19	0.39		2.17
Al/TPG40	2.22	0.50	0.17	0.39		3.28
Al/TPG40 with four converters	2.26	0.48	0.16	0.59		3.49
Be/TPG40	1.74	0.50	0.17	0.39		2.80
C-C/TPG40	1.88	0.49	0.17	0.39		2.93
Fixed heat-pipe location (14 cm)						
Al	3.28	0.33	0.38	0.39		4.38
C-C	1.39	0.33	0.21	0.39		2.32
Be	1.59	0.33	0.28	0.39		2.59
Al/TPG40	2.31	0.33	0.17	0.39		3.20
C-C/TPG40	1.94	0.33	0.17	0.39		2.83
No heat pipe						
Al/TPG65	1.78				0.20	1.98
C-C/TPG65	1.61				0.20	1.81
Be/TPG65	1.55				0.20	1.75
Al	3.81				0.20	4.01
Al with four converters	2.30				0.40	2.70
Be	2.00				0.20	2.20
Be with four converters	1.20				0.40	1.60
C-C	2.09				0.20	2.29

range of 30 to 1700 W/m-K. The radiator outer radius, mass, and temperature difference did not significantly change for thermal conductivities greater than 500 W/m-K.

9. Radiators for power systems with two and four Stirling converters (each system sized to meet the required 105-W_e power output 6 years after beginning of mission (BOM)) were compared for a radiator design with 0.40-volume fraction TPG, Al/TPG fins. The results were essentially identical for outer radius and temperature difference; the total radiator mass for the four-converter system was slightly heavier, 3.49 versus 3.28 kg.

No-Heat-Pipe Radiator Designs

1. Radiator fins directly coupled to the converter cold end have the advantages of eliminating the heat pipe and reducing the temperature difference between the converter cold-end temperature and the radiator fin root temperature. However, they do require heat to flow only radially outward from the converter cold end as opposed to the heat-pipe radiator designs that have heat flowing in both directions from the heat pipe. Thus, high thermal conductivity is more important for the no-heat-pipe designs. Flat, tapered, and parabolic cross sections of various materials were investigated.

2. For the no-heat-pipe radiators, the TPG designs provide clear advantages as compared with radiators that use fins of the pure materials. They are lighter and have significantly smaller size and maximum temperature difference. The total radiator mass varied from 1.75 kg for Be/TPG to 1.98 kg for Al/TPG. The outer radius was about 20.2 cm for each, and the maximum temperature differences were 14 to 15 K. The least-mass designs all used 0.65-volume fraction TPG, which was the lowest volume fraction evaluated (to maintain a minimal fin thickness of about 3 mm). Thermal conductivity was as high as 1228 W/m-K for C-C/TPG.

3. Tapered C-C fins were the best of the pure materials, having a total mass of 2.29 kg, an outer radius of 25.6 cm, and a maximum temperature difference of 59 K. Parabolic Be and Al fins both had outer radii of about 27.5 cm and maximum temperature differences of 76 K. The total mass was 2.20 kg with Be and 4.01 kg with Al. Both size and temperature difference could be reduced by increasing the fin thickness and mass.

4. Sensitivities to view factor, heat rejection, and converter cold-end temperature were determined for a radiator design with flat 0.65-volume fraction TPG, Al/TPG fins. Each significantly influenced the radiator size and mass. Again, for this study, view factor was the least known of these parameters. For a range of view factors from 1 to 2, the total radiator mass varied from 3.05 to 1.49 kg and the outer radius varied from 25.6 to 17.2 cm.

5. For a fixed fin thickness (2.903 mm) and density, the thermal conductivity was arbitrarily varied over a range of 200 to 10 000 W/m-K. The outer radius, mass, and temperature difference did not significantly change for thermal conductivities greater than 1000 W/m-K. To reduce the maximum temperature difference below 10 K, the thermal conductivity must be greater than 1700 W/m-K (for a fin thickness of 2.903 mm). This compares to a thermal conductivity of only 500 W/m-K needed for a heat-pipe radiator to reduce the maximum temperature difference below 7 K (for a total fin thickness, both fins, of 3.386 mm).

6. Radiators for power systems with two and four Stirling converters (each system sized to meet the required 105-W_e power output 6 years after BOM) were compared for radiator designs with Al and Be fins. With these lower conductivity materials, the smaller amount of rejected heat per converter with the four-converter system made a significant difference. For both Al and Be fins, the outer radius decreased from about 27.5 to 15.2 cm and the maximum temperature difference from 76 to 29 K. The total radiator mass was reduced from 4.01 to 2.70 kg for Al and from 2.2 to 1.6 kg for Be. A view factor of 1.5 was used for all these designs; this result has to be carefully analyzed because the radiators for the four-converter system may have a lower view factor than those for a two-converter system.

Comparison of Heat-Pipe and No-Heat-Pipe Designs

1. The least-mass no-heat-pipe designs are the lightest of all radiator concepts evaluated and had a minimum total radiator mass of 1.75 kg for 0.65-volume fraction TPG, Be/TPG. This design also had the smallest outer radius at 20.2 cm (in a plane perpendicular to the converter axes of symmetry). No-heat-pipe designs with C-C/TPG and Al/TPG fins were very similar in mass, size, and maximum temperature difference to the Be/TPG design. The lightest heat-pipe designs were with Be fins (2.17 kg) and C-C fins (2.24 kg) with optimized heat-pipe locations. The smallest outer radius for the heat-pipe designs was 29.2 cm (in the same plane as the converter axes of symmetry) for each of the designs with TPG fins and optimized heat-pipe locations.

2. View factors must be carefully calculated for given system and spacecraft layouts as they significantly affect radiator size and mass. For this study, comparisons of different materials and for heat-pipe versus no-heat-pipe designs were made for a constant view factor of 1.5.

3. The no-heat-pipe radiators were mounted orthogonal to the converter longitudinal axis whereas the heat-pipe radiators were mounted parallel to this axis. As such, a system with the no-heat-pipe radiators would require the power system to be mounted farther from the spacecraft. The no-heat-pipe radiators face each other and the radioisotope general purpose heat source (GPHS) and may require a cutout to allow the mechanical connection of the two opposed converters, if necessary, for minimizing vibrations.

Concluding Remarks

A radiator design and performance code GPHRAD was written to support Stirling radioisotope power systems for deep space missions. The code uses cylindrical coordinates to model the circular sector radiator surfaces; it solves the second-order, fourth-degree, finite-difference equations that are characteristic of radiating fins. A subprogram TSCALC is used to determine the background temperature of space. This sink temperature is the equilibrium temperature that a radiating surface would attain in the absence of internal heat generation. Accurate determination of this value for various missions and Solar System locations is a prerequisite for space radiator design. Sink temperature is a function of several input variables, notably the absorptivity/emissivity ratio of the radiator surface. Low values of this ratio (e.g., 0.18 for the coating Z–93) are important for minimizing the sink temperature. Low values of the resulting temperature difference across the radiator surface (a few tens of kelvin) are also important to prevent radiator coating degradation.

The GPHRAD code was used to screen many preliminary radiator designs. Two general concepts were studied: (1) heat-pipe designs and (2) no-heat-pipe disk designs mounted directly on the Stirling converter cold end. For each concept, both high-tech and state-of-the-art materials were used for the radiator fins. The high-tech material was encapsulated thermal pyrolitic graphite (TPG), which has a 1700-W/m-K thermal conductivity over four times that of copper. In this study, TPG encapsulated with aluminum (Al), beryllium (Be) or carbon-carbon (C-C) was used. State-of-the-art materials used for the fins included Al and Be. A C-C composite was also used and is discussed below as a state-of-the-art material, even though its use in space radiators is just beginning. The same is true for a new aluminum-beryllium alloy identified as AlBeMet.

For the heat-pipe designs, the required radiator surface area for a given heat load was primarily a function of heat-pipe radial position and fin thermal conductivity. The deviation from the optimum radial heat-pipe position (~70 percent of radial span) to a heat-pipe position matched the converter cold end (~40 percent of radial span) and resulted in radiator area penalties. These were only about 4 percent for TPG composites but were 20 percent for C-C, 50 percent for Be, and near 100 percent for Al. For a nominal 105-W_e power system, these heat-pipe designs had masses as low as 2.17 kg for optimal heat-pipe locations in state-of-the-art fin materials and had acceptable temperature differences (15 to 35 K). The TPG heat-pipe designs were 0.5 to 0.75 kg heavier than the state-of-the-art heat-pipe fin designs but had very low temperature differences (< 5 K).

The no-heat-pipe designs were driven by operational and design simplicity. These designs could eliminate any heat-pipe reliability concerns such as dryout during launch or orbital transfer phases or heat-pipe failure due to working fluid loss in case of micrometeoroid puncture. The no-heat-pipe designs included the lightest radiators that had TPG fins with masses as low as 1.75 kg and temperature differences of about 15 K. State-of-the-art C-C and Be designs had masses of only about 2.25 kg, but the temperature differences across the disks ranged from 60 to 76 K. The Be design temperature drop could be decreased from 75 K to a more acceptable 35 K with increased thickness at the inside diameter for a mass increase of about 1 kg (to ~3.2 kg). State-of-the-art Al designs would be almost 2 kg heavier than similar Be or C-C designs.

Several factors need further consideration before a choice of design concept is made. The no-heat-pipe fins are mounted in a plane that is orthogonal to the plane of the heat-pipe fins. Therefore, a power system with a no-heat-pipe radiator may need to be mounted farther from the spacecraft and could have different sensitivities to vibrations from one that has a heat-pipe radiator mounted in the plane of the fins. Also, since a radiator fin view factor of 1.5 was used for both heat-pipe and no-heat-pipe designs in the comparison study, a careful calculation of view factors for power system-spacecraft layouts of each concept is needed. Finally, the use of lightweight beryllium-aluminum alloys that combine desirable thermophysical properties of the two alloying elements should be considered.

Appendix A

Radiator Design and Analysis Code

This section summarizes the highlights of the procedure followed in developing the computational tool GPHRAD, including the subroutine TSCALC for the calculation of space sink temperatures. A brief description of code options, including the option for minimum mass achieved by optimizing heat source position, is also presented.

Radiator Code Development

As a point of departure, the first radiator geometry to be analyzed was the OSC power system concept shown in figure 1. The radiator consists of four pie-shaped segments mounted between adjacent Stirling converters. To match the circular quadrant radiator configuration, a quasi-two-dimensional, finite-difference code was written in cylindrical (polar r, θ, z) coordinates. A prime objective was to enable a complete parametric evaluation of a radiator concept using newly developed high-thermal-conductivity graphite material as reported by Montesano (ref. 11) and compare the resulting performance with other materials of lower conductivity. Pertinent parameters to be varied included panel thickness, thermal conductivity, heat rejection (i.e., converter cold end) temperature, view factor, and absorptivity/emissivity ratio. Note that the radial positioning of the heat pipe is also a critical variable.

The work on this code involved constructing a main program that made repeated calls on a coordinate-transformed (Cartesian-to-polar) radiating fin code (RADFIN) developed by Juhasz (ref. 10). The coordinate transformation also had to account for both radially outward and inward heat flows. Since each of these calls involves an iteration cycle, attention was paid to convergence criteria and relaxation algorithms to facilitate convergence for highly asymmetric geometries (i.e., where the heat source is located very close to the inner radius and far from the outer radius). To permit the inclusion of nonisotropic thermal conductivity, heat flow in the direction orthogonal to the radiator plane (z-direction) is also accounted for, as is the variation of radiator disk thickness. The derivation of governing equations and relationships in Cartesian coordinates for the second-order, fourth-degree ordinary differential equation (ODE) to be solved by finite-difference techniques is given in appendix B.

The computational tool GPHRAD for the design analysis of heat rejection system radiators for deep space probes is described in further detail by Juhasz, Tew, and Thieme (ref. 12). Its capabilities and options have recently been enhanced, and the code has been used for doing design tradeoff studies. This tool is especially useful for heat rejection subsystem studies for Stirling power systems with GPHS heat sources. The initial analysis capability was for radiator configurations that con-sisted of circular quadrants with heat pipes carrying the heat from the Stirling converter cold side to the radiator surface. With the recent enhancements, the code now has the capability to analyze the performance of a disk-shaped circular arc (of arbitrary included angle) and conical radiators assembled directly to the Stirling cold end in a plane perpendicular to the converter longitudinal axis. This approach eliminates the need for a heat pipe. As indicated above, heat flow and temperature distribution computations are performed in a polar coordinate system. The code also takes into account the radiator thickness in the orthogonal direction as a function of radial position. Thus, it is possible to analyze constant thickness as well as tapered and parabolic radiator designs to accomplish significant weight savings.

Equivalent Sink Temperature Calculations

For the calculation of equivalent sink temperature anywhere in the Solar System, a subroutine (TSCALC) takes into account the Sun-to-spacecraft distance; the angle at which the radiator surface intercepts the solar heat flux β_{ilum}; emissivity ε; absorptivity α; and view factor to space F. This sink temperature T_S, along with the radiator heat source temperature and thermophysical properties and geometry (thickness and taper) of the radiator material, are the inputs required by GPHRAD to calculate the area needed (i.e., radial dimensions) for a required heat rejection load. Radial temperature profiles, heat fluxes, and fin efficiencies are also computed and printed out.

Option for Minimum Radiator Area and Mass

An additional powerful option enables the code to perform an optimization (based on the calculus of variation techniques) to place the heat pipe in the radial position that will minimize the required radiator surface area and mass, subject to user-specified constraints. Among these constraints between the outer and inner radiator sectors are equal temperature drops, equal areas, or equal heat rejection loads. The latter constraint produces the overall minimum radiator area and mass.

The user can bypass this option and position the heat source arbitrarily, such as in a location convenient for assembly of the overall power system. By running the code successively under both options, the user can ascertain the radiator mass penalty due to not positioning the heat pipe at the optimum location. Results indicate that this penalty can be as high as 60 percent for low-thermal-conductivity materials (such as Al with a conductivity of 173 W/m-K). This penalty disappears for very high-

conductivity materials, such as TPG composites with composite thermal conductivity in the range of 1200 to 1300 W/m-K. Given that the high-thermal-conductivity encapsulated TPG material lessens the penalty of nonoptimum heat-pipe placement, several code test runs were initially made by the author (Juhasz) with the heat source (heat pipe) essentially at the inner radius of the disk giving encouraging results. These results suggested that the radiator inner radius may be mated directly to the converter cold end without a heat pipe, thus greatly simplifying design and fabrication and reducing cost. Moreover, operation in service, especially during the high-G launch and orbit transfer phases of the mission, would be improved along with reliability and survivability to foreign object damage during mission life.

Examples of GPHRAD Output Results

Sample code output cases for low- and high-thermal-conductivity radiator materials are shown in tables AI and AII, respectively. These cases were run prior to the runs made for this report and their masses are not typical of the radiator masses achieved in this study. Because of space limitations, these tables show summary results only; however, the code output also contains voluminous intermediate results that include core and surface radial temperature profiles for the outer sector (from the radiator heat source outward) and the inner sector (from the radiator heat source inward). Moreover, axial heat flux listings (into and out of the individual control

volumes) and a listing of heat radiated at each node are also included with numerical information regarding convergence criteria and convergence processes.

To aid the reader in interpreting the information presented in the tables, a few clarifying remarks are in order. The top line lists the radial dimensions of the radiator sector. In line two, RI refers to the inner radius, RM to the radius where the heat source is positioned, and RO to the outer radius. All dimensions are given in meters. The remaining information listed is self-explanatory, except for the acronyms INNER and OUTER DELTA R(MM) that refer to a control volume radial dimension determined by the number of node points (NP) specified by the user. Note that the overall results refer to the four-converter system configuration. The taper factor (ENDF) is the end point multiplier of the original thickness at RI and is equivalent to the tip-to-root thickness ratio. Thus, for a constant thickness, ENDF = 1, whereas ENDF = 0.1 would indicate a taper such that the thickness at the outer radius is only 10 percent of the thickness at the inner radius.

The radial temperature profiles for these cases are plotted in figure A1. Note that for the 50-W/m-K case, the maximum temperature occurs at the 27.3-cm location (location of the heat-pipe condenser), and the outer profile extends to the outer radius position of 37.3 cm. For the high-conductivity case, the outer radius is only about 34.5 cm, and the optimum heat-pipe location is at 24.6 cm. These coordinates reflect the lower radiator area required because of the higher effective radiator temperatures (lower temperature changes) achieved at the higher conductivity.

TABLE AI.—GPHRAD CODE OUTPUT SUMMARY FOR LOW-THERMAL-CONDUCTIVITY
RADIATOR MATERIAL
[k = 50 W/m-k.]

```
          90 DEGREE SECTOR RESULTS


RI(M) = 0.05 ; RM(M) = 0.2732409008 ; RO(M) = 0.3736034218


FIN ROOT/HP TEMP(K) =   400.0; SINK TEMP(K) =   222.5
 EFFECTVE RAD.TEMP(K) =   383.9
THERMAL CONDUCTIVITY (W/MK) =    50.0; VIEW FACTOR (FV) =    1.50


QTOT (WATTS) =   150.00        SAIL-AND RADIATING AREA (M2) =   .1077   .1615


 INNER DELTA R(MM) =   2.232 ; OUTER DELTA R(MM) =    1.004 ; NODES (NP) =   100


OUTER SECTOR QR(WATTS) =    75.01 ; INNER SECTOR QR(WATTS) =   74.99
OUTER SECTOR DELTAT (K) =   16.2  ; INNER SECTOR DELTAT (K) =   38.0
OUTER SECTOR FIN EFFIC. = .87929 ; INNER SECTOR FIN EFFIC. =   .7908


     OVERALL RESULTS : - TOTAL RADIATOR MASS (KG) =    9.69
                      RADIATOR SPECIFIC MASS(KG/M2) =   15.00
TOTAL HEAT RADIATED(WATTS) =     600.0; TOTAL RADIATOR SAIL AREA(M2) =    .4306
   NUMBER OF STIRLING UNITS =      4  ;    TOTAL RADIATING AREA(M2) =    .6460
 MATERIAL DENSITY (CM/CC) = 2.10;     RADIATOR THICKNESS(MM) = 10.00
                                      TAPER FACTOR (ENDF) =   1.00
HT PIPE CONDENSER HEAT FLUX (W/CM2) =  1.11; FVEXP =    1.00
                    HT PIPE MASS (KG) =     .64; SPEC.MASS- (G/CM-HPSPW) =   3.75
 TOTAL EXECUTION TIME = 37.46 SEC
```

TABLE AII.—GPHRAD CODE OUTPUT SUMMARY FOR HIGH-THERMAL-CONDUCTIVITY
RADIATOR MATERIAL
[k = 500 W/m-k.]

```
        90 DEGREE SECTOR RESULTS


RI(M) = 0.05 ; RM(M) = 0.2470911376 ; RO(M) = 0.3449148423


FIN ROOT/HP TEMP(K) =  400.0; SINK TEMP(K) =  222.5
 EFFECTVE RAD.TEMP(K) =  398.2
THERMAL CONDUCTIVITY (W/MK) =  500.0; VIEW FACTOR (FV) =   1.50


QTOT (WATTS) =  150.00       SAIL-AND RADIATING AREA (M2) =  .0915  .1372


 INNER DELTA R(MM) =  1.971 ; OUTER DELTA R(MM) =    .978 ; NODES (NP) =  100


OUTER SECTOR QR(WATTS) =   75.00 ; INNER SECTOR QR(WATTS) =   75.01
OUTER SECTOR DELTAT (K) =   1.8  ; INNER SECTOR DELTAT (K) =   4.1
OUTER SECTOR FIN EFFIC. = .98542 ; INNER SECTOR FIN EFFIC. =   .9748


     OVERALL RESULTS : - TOTAL RADIATOR MASS (KG) =   8.27
                 RADIATOR SPECIFIC MASS(KG/M2) =  15.06
TOTAL HEAT RADIATED(WATTS) =    600.0; TOTAL RADIATOR SAIL AREA(M2) =   .3659
  NUMBER OF STIRLING UNITS =     4   ;     TOTAL RADIATING AREA(M2) =   .5488
  MATERIAL DENSITY (GM/CC) = 2.10;     RADIATOR THICKNESS(MM) = 10.00
                                          TAPER FACTOR (ENDF) =  1.00
HT PIPE CONDENSER HEAT FLUX (W/CM2) =  1.23; FVEXP =   1.00
                  HT PIPE MASS (KG) =    .58; SPEC.MASS- (G/CM-HPSPW) =  3.75
   TOTAL EXECUTION TIME = 10.54 SEC
```
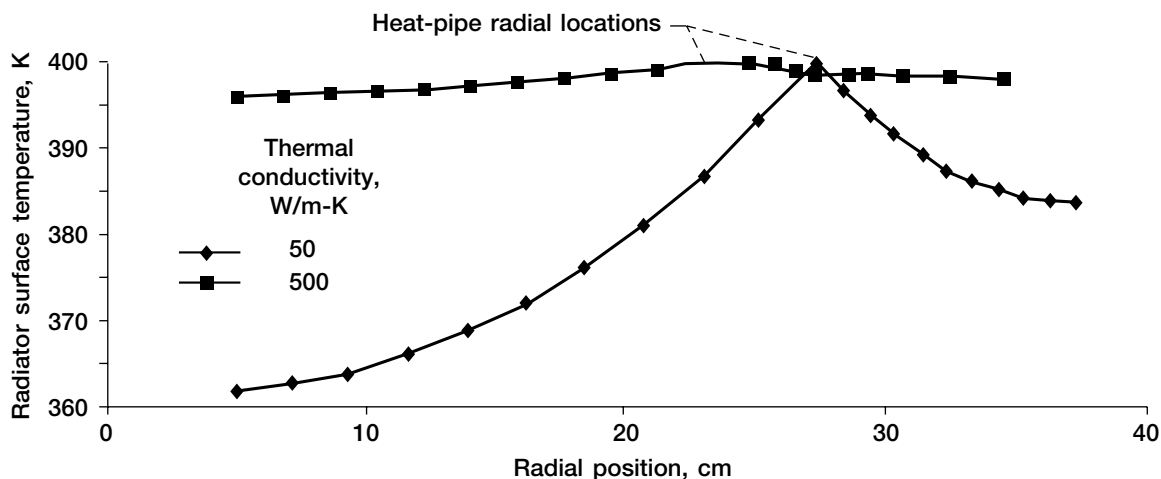

Figure A1.—Typical GPHS-Stirling radiator temperature profiles for two thermal conductivities
of radiator material. Radiator heat rejection, 600 W$_t$; view factor, 1.5; sink temperature, 223 K;
emissivity, 0.85; radiator fin thickness, 0.01 m.

Appendix B

Analysis of Heat Transfer From a Radiating Fan

In performing this analysis, consider the one-dimensional conduction and radiation heat transfer processes (fig. B1). The accompanying table gives the nomenclature for the variables that are essential to the derivation of the characteristic ordinary differential equation governing the heat transfer.
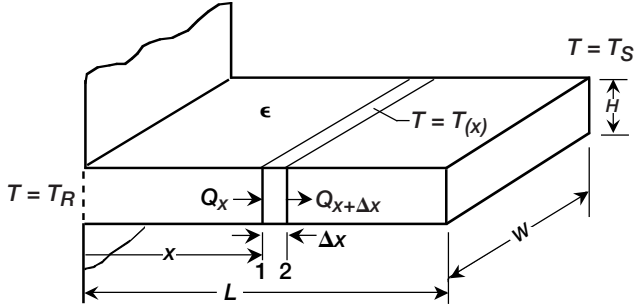

Figure B1.—Nomenclature for radiating fin heat transfer analysis.

A_C .... cross-sectional area, m^2
A_S .... surface area, m^2
F .... view factor
H .... fin thickness, m
k .... thermal conductivity, W/m-K
L .... fin length, m
Q .... heat rejection, W_t
T .... fin wall temperature, K
T_R .... root temperature, K
T_S .... sink temperature, K
W .... fin width, m
ε .... surface emissivity
σ .... Stefan-Boltzmann constant, 5.67×10^{-8} W/$m^2$$K^4$

Note that the longitudinal dimension in the direction of heat flow (the fin root-to-tip dimension) is designated L, with the variable dimension designated x, where $0 < x < L$.

At any section x $(0 < x < L)$,

$$Q_x = kA \frac{dT_1}{dx} \qquad (B1)$$

where

$$A = A_C = H \times W$$

and

$$Q_{x+\Delta x} = -kA \frac{dT_2}{dx} \qquad (B2)$$

Also

$$(Q_x) - (Q_{x+\Delta x}) = \sigma \varepsilon F A_S \left(T^4 - T_S^4 \right) \qquad (B3)$$

where

$$A_S = W \times \Delta x$$

or

$$-kHW \left(\frac{dT_1}{dx} - \frac{dT_2}{dx} \right) = \sigma \varepsilon F W \Delta x \left(T^4 - T_S^4 \right) \qquad (B4)$$

Dividing through by $W\Delta x$ and letting Δx approach zero, equation (B4) can be rewritten as an ordinary differential equation of the second order, fourth degree:

$$kH \frac{d^2 T}{dx^2} + \sigma \varepsilon F \left(T^4 - T_S^4 \right) = 0 \qquad (B5)$$

With boundary conditions,

$$T = T_R \qquad \text{at} \quad x = 0 \qquad (B6)$$

$$-kH \frac{dT}{dx} = \sigma \varepsilon F \left(T_L^4 - T_S^4 \right) \qquad \text{at} \quad x = L \qquad (B7)$$

or considering the last control volume,

$$Q_{\text{CONDUCTED IN}} = Q_{\text{RADIATED OUT}} \qquad (B8)$$

With T_L unknown, the solution of equation (B5) under boundary conditions (B6) and (B7) was accomplished by generating a finite-difference computer program with an arbitrary number of control volumes. This program was then exercised in an iterative mode to accomplish boundary condition (B7) within a specified tolerance (0.01 W) at the last control volume.

Aside from the fact that a closed-form analytical solution does not exist, a significant advantage of the numerical solution technique is that the fin cross-sectional area can be specified to vary according to a prescribed polynomial relationship. This capability is illustrated by the fin temperature profile results in figure B2 for a constant cross-sectional rectangular fin geometry profile and in figure B3 for a variable cross-sectional parabolic fin geometry. Numerical values for key input variables are shown in the (b) legends for these figures and have units consistent with those defined for figure B1. As expected, because of incremental heat radiation from the fin surface, the temperature gradient decreases with fin length for a rectangular fin geometry but is constant for the parabolic fin, resulting in a linear temperature profile. This is consistent for convectively cooled fins for which closed-form solutions do exist. Future work in this area will focus on combined radiation and convection.
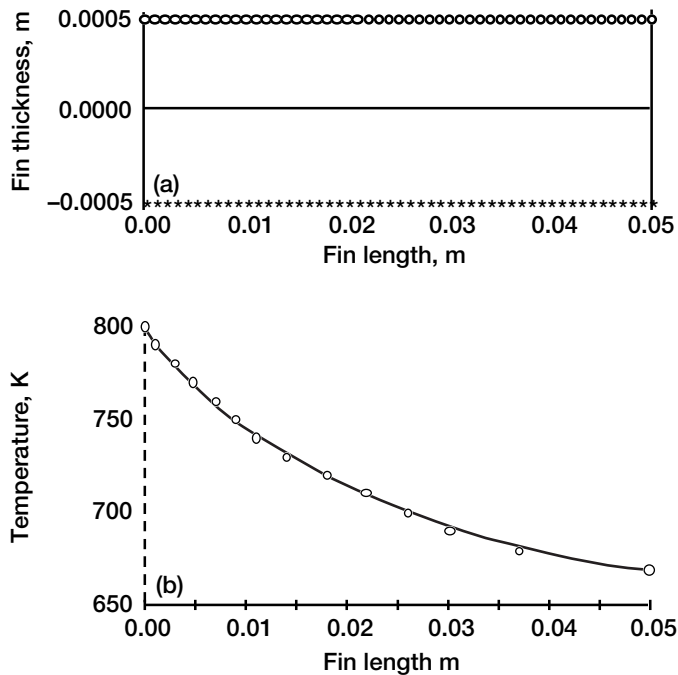
Figure B2.—Rectangular fin radiation heat transfer.
(a) Fin geometry profile. (b) Fin temperature profile
for thermal conductivity of 200, surface emissivity of
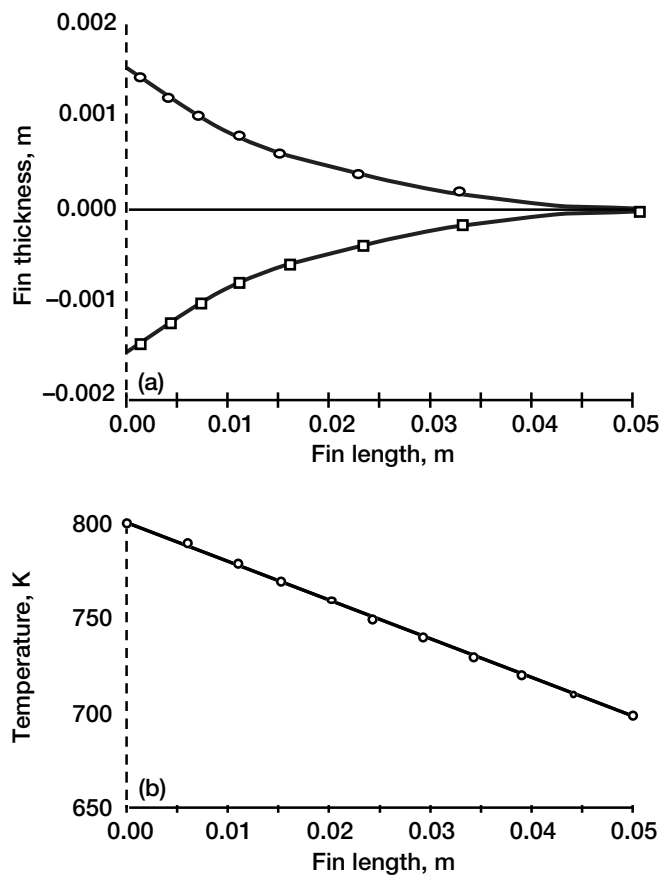0.85, view factor of 1.0, sink temperature of 230 K.

Figure B3.—Parabolic fin radiation heat transfer. (a) Fin
geometry profile. (b) Fin temperature profile for thermal
conductivity of 200, surface emissivity of 0.85, view
factor of 1.0, sink temperature of 230 K.

References

1. Frazier, T.A.: Advanced Conversion Technology Review Panel Report. Proceedings of the 33rd Intersociety Energy Conversion Engineering Conference, IECEC Paper 98–398, 1998.
2. Mondt, J.F.; and Nesmith, B.J.: Advanced Converter Technology Evaluation and Selection for ARPS; Advanced Radioisotope Power Source. Proceedings of the Space Technology and Applications International Forum, American Institute of Physics, Woodbury, NY, 1998.
3. Schock, A.; Or, C.T.; and Kumar, V.: Radioisotope Power System Based on Derivative of Existing Stirling Engine. Proceedings of the 30th Intersociety Energy Conversion Engineering Conference, vol. 1, ASME, New York, NY, 1995, pp. 649–656.
4. Schock, A.; Or, C.T.; and Kumar, V.: Radioisotope Power System Based on Improved Derivative of Existing Stirling Engine and Alternator. Proceedings of the Space Technology and Applications International Forum, American Institute of Physics, Woodbury, NY, 1999.
5. White, M.A., et al.: Status of an Advanced Radioisotope Space Power System Using Free-Piston Stirling Technology. Proceedings of the 33rd Intersociety Energy Conversion Engineering Conference, IECEC Paper 98–417, 1998.
6. White, M.A., et al.: Technology Demonstration of a Free-Piston Stirling Advanced Radioisotope Space Power System. Proceedings of the Space Technology and Applications International Forum, American Institute of Physics, Woodbury, NY, 1999, pp. 1413–1419.
7. Erbeznik, R.M.; and White, M.A.: Test Results and Commercialization Plans for Long Life Stirling Generators. Proceedings of the 31st Intersociety Energy Conversion Engineering Conference, vol. 2, Institute of Electrical and Electronics Engineers, Piscataway, NJ, 1996, pp. 1265–1270.
8. Juhasz, A.J.; and Peterson, G.P.: Review of Advanced Radiator Technologies for Spacecraft Power Systems and Space Thermal Control. NASA TM–4555, 1994.
9. Juhasz, A.J.; and Rovang, R.D.: Composite Heat Pipe Development Status: Development of Lightweight Prototype Carbon-Carbon Heat Pipe With Integral Fins and Metal Foil Liner. NASA TM–106909, 1995.
10. Juhasz, A.J.: Design Considerations for Lightweight Space Radiators Based on Fabrication and Test Experience with a Carbon-Carbon Composite Heat Pipe. NASA/TP–1998-207427, 1998. (PDF available online: ftp://ftp-letrs.lerc.nasa.gov/LeTRS/reports/1998;TP-1998.207427.pdf).
11. Montesano, Mark: New Material for Thermal Management has Four Times Thermal Conductivity of Copper. Materials Technology, vol. 11, no. 3, 1996.
12. Juhasz, Albert J., Tew, Roy C., and Thieme, Lanny G.: Design and Analysis Code for Heat Pipe Radiators of Stirling Power Systems Applicable to Deep Space Probes. Proceedings of the 11th International Heat Pipe Conference (Tokyo, Japan), Sept. 1999.

REPORT DOCUMENTATION PAGE

1. AGENCY USE ONLY *(Leave blank)*	2. REPORT DATE June 2000	3. REPORT TYPE AND DATES COVERED Technical Paper

4. TITLE AND SUBTITLE

Parametric Study of Radiator Concepts for a Stirling Radioisotope Power System Applicable to Deep Space Missions

6. AUTHOR(S)

Albert J. Juhasz, Roy C. Tew, and Lanny G. Thieme

5. FUNDING NUMBERS

WU–632–1A–1G–00

7. PERFORMING ORGANIZATION NAME(S) AND ADDRESS(ES)

National Aeronautics and Space Administration
John H. Glenn Research Center at Lewis Field
Cleveland, Ohio 44135–3191

8. PERFORMING ORGANIZATION REPORT NUMBER

E–11717

9. SPONSORING/MONITORING AGENCY NAME(S) AND ADDRESS(ES)

National Aeronautics and Space Administration
Washington, DC 20546–0001

10. SPONSORING/MONITORING AGENCY REPORT NUMBER

NASA TP—2000-209676

11. SUPPLEMENTARY NOTES

Responsible person Albert J. Juhasz, organization code 5440, 216–433–6134.

12a. DISTRIBUTION/AVAILABILITY STATEMENT

Unclassified - Unlimited
Subject Categories: 18, 20, and 64   Distribution: Standard

Available electronically at http://gltrs.grc.nasa.gov/GLTRS

This publication is available from the NASA Center for AeroSpace Information, 301–621–0390.

12b. DISTRIBUTION CODE

13. ABSTRACT *(Maximum 200 words)*

Utilizing an in-house-developed, finite-difference (FD) computer code (GPHRAD with subprogram TSCALC), a large number of preliminary radiator designs were studied for Stirling/linear alternator power systems with general purpose heat sources (GPHS). These power systems are being evaluated as alternatives to radioisotope thermoelectric generators (RTG's) for deep space missions. System nominal electric power output was 105 W (105 W_e) at an average conversion efficiency of 22 percent over the lifetime of the mission. The nonconvertible heat of 371 W at the cycle cold temperature was the input heat load to the GPHRAD code. This code was written in cylindrical polar coordinates for efficient analysis of heat rejection to a space sink temperature by means of one or more circular-sector radiators, with or without heat pipes. The following materials of fabrication were considered: aluminum, beryllium, carbon-carbon (C-C), and encapsulated thermal pyrolytic graphite (TPG), an advanced high-thermal-conductivity material currently being evaluated for space applications. Results of the study showed the effect of key parameters on radiator area and mass. Among these parameters, thermal conductivity, material density, heat-pipe radial location, radiator surface coating, and the use of trapezoidal or parabolic tapers for the radiator disk sectors were the most significant. Furthermore, radiators based on no-heat-pipe designs would be immune to evaporator dryout at launch and to onboard propulsion system firings during the mission. Moreover, they would not be adversely affected by micrometeoroid impact and would also have lower fabrication costs.

14. SUBJECT TERMS

Space radiator; Computer code; Heat-pipe radiator

15. NUMBER OF PAGES
38

16. PRICE CODE
A03

17. SECURITY CLASSIFICATION OF REPORT Unclassified	18. SECURITY CLASSIFICATION OF THIS PAGE Unclassified	19. SECURITY CLASSIFICATION OF ABSTRACT Unclassified	20. LIMITATION OF ABSTRACT